TU Delft

Delft University of Technology

Document Version
Final published version

Licence
CC BY

Citation (APA)
Overes, P. H. P., Borsje, B. W., Luijendijk, A. P., Tam, Z., Bloem, C. M. A., & Hulscher, S. J. M. H. (2026). How 3D Processes Drive Trench Infill and Sand Wave Regeneration After Dredging. *Journal of Geophysical Research: Earth Surface*, *131*(10), Article e2025JF008603. https://doi.org/10.1029/2025JF008603

Important note
To cite this publication, please use the final published version (if applicable).
Please check the document version above.

Copyright
In case the licence states “Dutch Copyright Act (Article 25fa)”, this publication was made available Green Open Access via the TU Delft Institutional Repository pursuant to Dutch Copyright Act (Article 25fa, the Taverne amendment). This provision does not affect copyright ownership.
Unless copyright is transferred by contract or statute, it remains with the copyright holder.

Sharing and reuse
Other than for strictly personal use, it is not permitted to download, forward or distribute the text or part of it, without the consent of the author(s) and/or copyright holder(s), unless the work is under an open content license such as Creative Commons.

Takedown policy
Please contact us and provide details if you believe this document breaches copyrights.
We will remove access to the work immediately and investigate your claim.

This work is downloaded from Delft University of Technology.

Check for updates

JGR Earth Surface

RESEARCH ARTICLE
10.1029/2025JF008603

How 3D Processes Drive Trench Infill and Sand Wave Regeneration After Dredging

Pauline H. P. Overes[1,2], Bas W. Borsje[1], Arjen P. Luijendijk[2,3], Zeta Tam[2,3], Celine M. A. Bloem[3], and Suzanne J. M. H. Hulscher[1]

[1]University of Twente, Marine and Fluvial Systems, Enschede, The Netherlands, [2]Deltares, Delft, The Netherlands, [3]Faculty of Civil Engineering and Geosciences, Delft University of Technology, Delft, The Netherlands

Key Points:

- Surrounding bathymetry highly affects current patterns and sediment distribution within the trench, leading to amplified sand wave regrowth
- Tidal currents drive trench infilling through bed slope-induced transport, while storm-induced currents can lead to asymmetrical infilling
- Infill rates are highly sensitive to trench side-slope steepness and less to trench width

Supporting Information:

Supporting Information may be found in the online version of this article.

Correspondence to:

P. H. P. Overes,
p.h.p.overes@utwente.nl;
pauline.overes@deltares.nl

Citation:

Overes, P. H. P., Borsje, B. W., Luijendijk, A. P., Tam, Z., Bloem, C. M. A., & Hulscher, S. J. M. H. (2026). How 3D processes drive trench infill and sand wave regeneration after dredging. *Journal of Geophysical Research: Earth Surface*, *131*, e2025JF008603. https://doi.org/10.1029/2025JF008603

Received 2 JUN 2025
Accepted 16 SEP 2026

Author Contributions:

Conceptualization: Pauline H. P. Overes, Bas W. Borsje, Arjen P. Luijendijk, Zeta Tam, Celine M. A. Bloem, Suzanne J. M. H. Hulscher
Data curation: Pauline H. P. Overes
Formal analysis: Pauline H. P. Overes, Zeta Tam, Celine M. A. Bloem
Funding acquisition: Bas W. Borsje, Arjen P. Luijendijk, Suzanne J. M. H. Hulscher
Investigation: Pauline H. P. Overes, Zeta Tam, Celine M. A. Bloem

© 2026 The Author(s). Journal of Geophysical Research: Earth Surface published by Wiley Periodicals LLC on behalf of American Geophysical Union. This is an open access article under the terms of the Creative Commons Attribution License, which permits use, distribution and reproduction in any medium, provided the original work is properly cited.

Abstract Dynamic bedforms, such as sand waves, may pose a threat to offshore energy infrastructure. Due to their impact on seabed mobility, dredging is often required to reduce risks, for example, to avoid cable exposure. However, commonly used data-driven methods cannot predict the evolution of partially dredged sand waves. Therefore, we apply a high-resolution Delft3D FM model to reproduce the measured morphological evolution of a dredged cable trench through sand waves and quantify the 3D interactions between the dredged area and surrounding sand waves. Our simulations confirm that sand wave regrowth is driven by tide-averaged vertical circulation. Remarkably, these circulation cells persist even over a flat trench bed because of the influence of adjacent nondredged sand waves. Trench infill results from gravitational modification of bed-load transport over the trench side slopes, causing amplification, damping, and deflection of sediment transport. Because infill volume rates depend on slope steepness, sedimentation varies over time as slopes flatten and spatially with the surrounding sand-wave bathymetry. In contrast to side-slope steepness, trench width has little effect on infill volume rates. Temporal variations in the trench infill clearly follow the spring-neap cycle. Although storm-induced currents did not significantly increase trench infill rates, they cause preferential infilling on one side by altering tide-induced transport asymmetry. The model reproduces the multiyear sediment balance over the trench well, with default model settings, showing its potential predictive capabilities. These process-based insights help explain differences in recovery timescales between environments and trench designs.

Plain Language Summary Sand waves are dynamic bedforms on the seabed, which can pose a threat to offshore infrastructure due to the variation in seabed level over time related to their movement. To ensure safety of infrastructure, oftentimes part of the sand wave is dredged away. However, state-of-the-art predictive tools are unable to tackle the dynamics of these complex systems. Therefore, we have set up a detailed computer model (Delft3D FM) to simulate and understand how a dredged trench through sand waves recovers. The model reveals 3-dimensional interactions between the dredged trench and the surrounding sand waves, such as sideways infilling driven by the steep side-slopes of the trench. Within the trench the current patterns match those found over a sand wave field, even if the sand waves are no longer present. This leads to faster regrowth of the sand waves. Tidal currents are the main driver of trench infill. The currents induced by storms can influence the location where the sediment ends up, possibly leading to movement of the trench over time. The model reproduced measured changes well. These findings help us understand the recovery processes of trenches through sand wave fields, which supports better planning and safer design of offshore infrastructure.

1. Introduction

Over the past decades the offshore area has become an integral part of our energy, food and transportation system. Shallow continental shelf areas are found to be highly suitable for, among others, green energy production and sand mining. Especially on these shallow, sandy shelf areas, often dynamic bed forms are encountered. These dynamic bedforms, such as tidal sand waves, may pose a threat to offshore infrastructure, due to the changes in seabed level related to their dynamics. To accommodate offshore developments in sand wave areas, bed level predictions over decadal timescales are thus required. Moreover, their dynamics regularly raise the need for dredging before cable installation to avoid future exposure (Németh et al., 2003). To support offshore developments in sand wave areas we thus need to increase our understanding of seabed dynamics and the impact of dredging in the offshore environment on the timescale of years to decades.

Methodology: Pauline H. P. Overes, Zeta Tam, Celine M. A. Bloem
Project administration: Suzanne J. M. H. Hulscher
Software: Pauline H. P. Overes, Zeta Tam, Celine M. A. Bloem
Supervision: Bas W. Borsje, Arjen P. Luijendijk, Suzanne J. M. H. Hulscher
Validation: Pauline H. P. Overes
Visualization: Pauline H. P. Overes
Writing – original draft: Pauline H. P. Overes
Writing – review & editing: Bas W. Borsje, Arjen P. Luijendijk, Zeta Tam, Celine M. A. Bloem, Suzanne J. M. H. Hulscher

Tidal sand waves, also known as marine dunes, are large-scale, rhythmic bed forms, which are formed due to complex interactions between tidal currents and seabed morphology (Hulscher, 1996), and can be found throughout the world at shallow sandy seabeds (e.g., Bao et al., 2014; Creane et al., 2022; Pessanha et al., 2023). Over time, these sand waves may migrate and change in shape, which combined with their substantial size can cause significant variations in local bed levels. Sand wave heights can reach up to 25% of the local water depth, while lengths are in the order of 100–1,000 m (Damen et al., 2018; Van Landeghem et al., 2009). Their migration rate can vary greatly between sites, with maxima of up to tens of meters per year (Creane et al., 2022; Van der Meijden et al., 2023). In the Southern North Sea sand wave migration rates are typically in the order of several meters per year.

Nowadays often data-driven analysis, based on historic bathymetry measurements, is applied to predict future bed levels in sand wave areas (Deltares, 2016). However, this type of analysis is unsuitable for dealing with changes in the system, for example, as a result of dredging, since this can disturb ongoing morphodynamic trends (Krabbendam et al., 2022). Moreover, areas where dredging has taken place are often closed for further measurements by public agencies, thereby limiting the available data for the development of conceptual models and system understanding. To gain understanding about the complex interactions between sand wave dynamics and dredged areas, we should thus look to other methods, such as process-based numerical models.

Process-based numerical models have been applied to predict and understand the response of the sand wave system to dredging interventions. Campmans et al. (2021) simulated the recovery of sand waves after various types of dredging interventions in an idealized sand wave system. They found that the recovery timescale of sand waves depends on the magnitude of the intervention volume as well as the type of intervention. Moreover, the sand wave amplitude change over time from the simulations was well described by a fitted Landau equation as proposed by Knaapen and Hulscher (2002), with the exception of some quicker recovery immediately after the intervention. The model can therefore be used to evaluate the efficiency of different dredging strategies. However, since the model only includes one horizontal dimension, perpendicular to the sand wave crests, the sand wave bathymetry and intervention are assumed to be unchanging in along-crest direction. In such a 2 Dimensional Vertical (2DV) model, with an in theory infinitely long intervention, there are no 3D interactions, such as sideways infilling of the dredged area, while dredging interventions often have a finite nature.

To forecast the development of a dredged cable trench, with a finite width, a high-resolution 3D model is required. Various studies have hinted at complex interactions between the surrounding sand waves and the dredged area, which cannot be captured in a simplified 2DV model. Orsted (2018), for example, reported significant deviations in the recovery rates of adjacent sand waves, as well as lateral migration of the trench after dredging. Moreover, the repeatedly observed lowering of the surrounding sand waves indicates side-ways infilling of the trench. In Larsen et al. (2020) one of the recovering sand waves grew back under a different angle, thereby forming two new crests from the different sides of the trench. Due to the high frequency of measurements after the intervention, Larsen et al. (2020) were able to track the recovery rate of the sand waves over time. They found that first there is a period with limited sand wave recovery, which they named the adaption period, followed by the regeneration period, in which the sand waves are regenerating. This adaption period has a duration in the order of weeks to months in the areas included in the study. These observations do not align with the quick recovery just after intervention found in the simulations by Campmans et al. (2021). These differences may be explained by the difference in dredging strategy, since a small part of the sand wave structure remains intact for the swiping strategy applied by Campmans et al. (2021). However, this could also be due to the exclusion of 3D processes in the 2DV model set-up.

With recent advances in computational power and model efficiency, the high-resolution 3D models needed to simulate trenched sand waves, are now within reach. This allows us to simulate multiyear morphological development of trenched sand waves, something that has not been done before. Using these simulations we can see how the dominant processes driving and dampening sand wave growth are affected by the dredging intervention. In bed load dominated settings these processes are tide-averaged vertical current circulation, driving net up-slope transport, and gravitational bed slope-induced transport, driving net down-slope transport, respectively (Borsje et al., 2014). Especially gravitational slope-induced amplification, dampening and deflection of bed load transport will also be of importance for interaction between the dredged and non-dredged areas, and thereby the infilling of the trench. A correct representation and parameterization of this process is thus vital for reproducing the morphological development of the trench. Increasing our understanding of these processes and their

21699011, 2026, 10, Downloaded from https://agupubs.onlinelibrary.wiley.com/doi/10.1029/2025JF008603 by Technical University Delft, Wiley Online Library on [14/10/2026]. See the Terms and Conditions (https://onlinelibrary.wiley.com/terms-and-conditions) on Wiley Online Library for rules of use; OA articles are governed by the applicable Creative Commons License

21699011, 2026, 10, Downloaded from https://agupubs.onlinelibrary.wiley.com/doi/10.1029/2025JF008603 by Technical University Delft, Wiley Online Library on [14/10/2026]. See the Terms and Conditions (https://onlinelibrary.wiley.com/terms-and-conditions) on Wiley Online Library for rules of use; OA articles are governed by the applicable Creative Commons License

dependence on the 3D morphology and hydrodynamics will help us determine the influence of trench design on the infill and regrowth rates.

The aim of this study is to identify the physical processes which play a role in the hydrodynamics and sediment transport and quantify the contributions of these processes to the multiyear trench infill and sand wave volume regeneration after dredging. To this end we will apply the process-based Delft3D Flexible Mesh (FM) model. Through simulations we will pay attention to the impact of different hydrodynamic conditions on short timescales (tidal cycles) as well as long-term (multi-year) morphological development using realistic hydrodynamics.

2. Methods

2.1. Field Site

For this study a field site on the Belgian Continental Shelf has been selected where in the spring of 2018 a 20 m wide cable trench was dredged through a field of sand waves, with wavelengths of 200–300 m and heights up to 8 m, removing everything above trough level. Subsequently sand wave regeneration is observed over a period of years. At this site Multi Beam Echo Sounder bathymetry measurements are available at four moments in time, spanning 5 years in total. These bathymetric measurements include two field surveys from the Flemish government from November 2016 and July 2021 (Agentschap Maritieme Dienstverlening en Kust, 2025). Moreover, in January and April 2018, the seabed surrounding the trench location was surveyed before and after the dredging. These in- and out-surveys have a width of 180 and 80 m respectively (Figure 1). All of the measurements have a resolution of 1×1 m. The application of this bathymetric field data allows for comparison of the morphological model results with the observed morphodynamics after the intervention.

In the considered area no hydrodynamic measurements are available. Alternatively, insight on the local hydrodynamics is gained from the Dutch Continental Shelf Model (DCSM) which includes both tidal forcing and other forcing mechanisms like atmospheric pressure, wind and density differences, and is extensively validated using measured hydrodynamics, see Deltares (2018). Using this model tidal and non-tidal currents in this area over the period from April 2018 until July 2021 were analyzed. The mean and maximum depth averaged current velocity due to tides are around 0.8 and 1.15 m/s respectively and the major axis of the tidal ellipse has an inclination of 53 °N. The ebb tidal currents, toward the south-west, are dominant in this region, with a difference in peak tidal current of on average 0.05 m/s. The maximum amplitude of the water level elevation due to tides (i.e., the difference between Lowest Astronomical Tide and Mean Sea Level) is 2.46 m. Especially atmospheric pressures and wind forcing cause deviations from these tidal hydrodynamics in this region. The average residual current is 0.035 m/s in flood direction (toward the north–east). There is a seasonality in the residual current strengths, with on average twice as strong residual currents during the stormy winter season. Of the 5% strongest currents 85% is aligned with the flood direction, with a maximum current strength of 1.2 m/s.

The two largest sand bodies in the sand wave pattern were chosen for further analysis and subsequent simulations. These sand waves have a very asymmetrical (asymmetry index ($A = [L_{\text{gentle}} - L_{\text{steep}}]/L$) of 0.5–0.8, depending on defined trough locations) and pointy shape, with a wavelength of 200–300 m and an undisturbed wave height of 7–8 m. Before the trench installation, the sand waves are observed to be migrating in ebb direction, toward the south-west, with a rate of a few meters per year. This migration can be explained by the dominance of the ebb tidal currents in this region. The steepest slopes of the sand waves are found facing the flood current, with a maximum steepness of up to 20° before dredging. Although the crests are quite straight at the location of the trench, with an orientation of approximately 160 °N, toward the north the crests show some curvature. This curvature possibly occurs under the influence of the West Hinder sand bank located at a few kilometers distance to the north-east of the sand wave area.

The trench was dredged to allow for the installation of the NEMO-link submarine power cable, which connects the electricity grids of Belgium and the UK. The trench crosses the sand waves approximately perpendicular to their crests. The local orientation of the trench is around 67.5 °N (Figure 1). The bottom of the trench, which has a width of approximately 20 m, is situated around the trough level of the sand waves (PMSS, 2013). Slopes of maximum 12° (1:5) steepness connect the trench bottom to the surrounding seabed, leading to a significantly wider dredged area at the location of the sand wave crests.

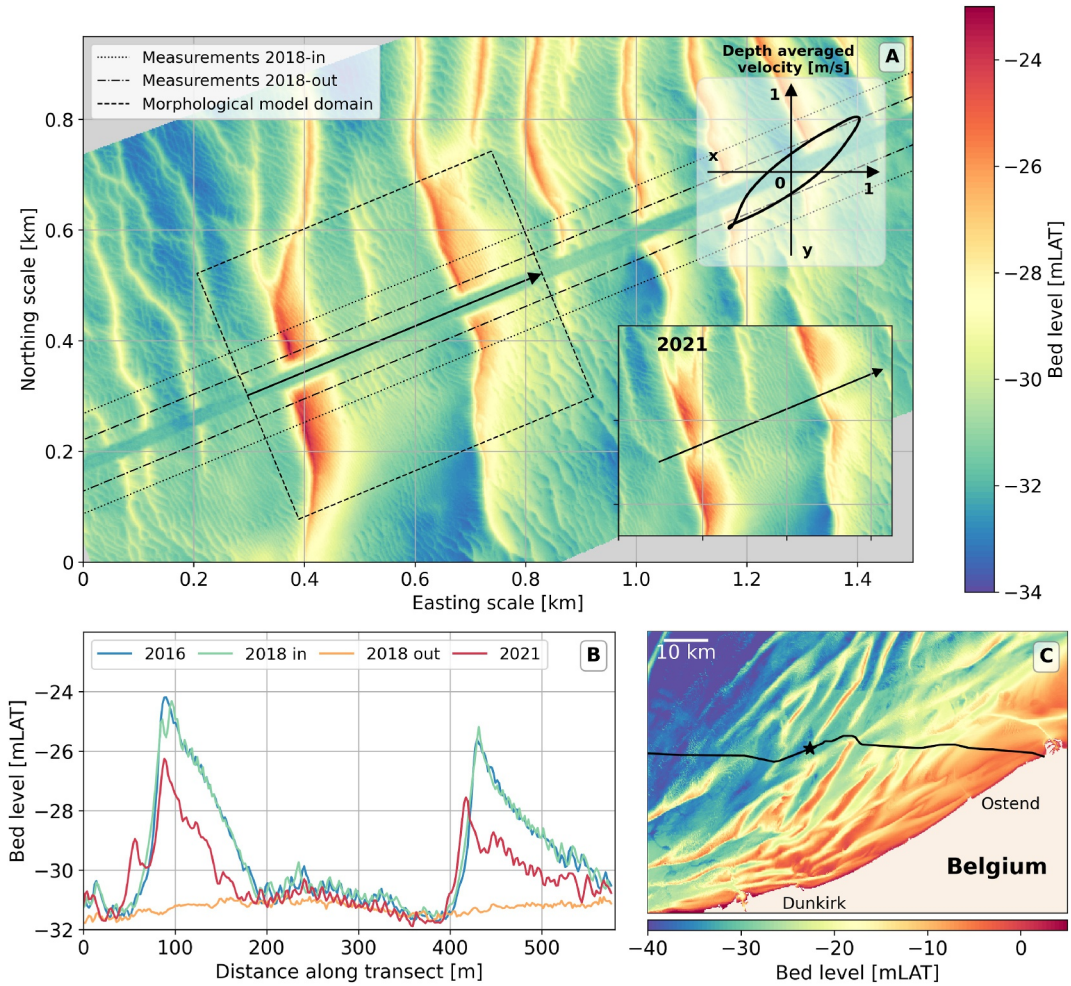


Figure 1. (a) Combined measured bathymetry: 2018-out survey, 2018-in survey and 2016 survey, with overlain plots: 2021 survey (lower) and representative tidal current velocities (upper). (b) Measured bathymetry along center line of trench (see arrow for location). (c) Large scale bathymetry from EMODNET (EMODnet (2024)) including location of field site.

The dredging clearly had a large impact on the sand wave morphology. The observed bathymetry from 2021, three years after installation, show that although in the trench the sand waves are recovering, the height of the surrounding sand waves has decreased. Moreover, the western sand wave shows a different migration rate for the area south and north of the trench, which leads to a separation of the regrowing crests. The largest bed level changes are found at the former crest locations. Over the 3.3 years measurement period, the sand waves have recovered approximately two thirds of their original crest height. The steep slopes facing the flood direction have recovered with the same steepness as before the intervention, while the gentle slopes are still somewhat lagging behind.

2.2. Modeling Software

The process-based Delft3D Flexible Mesh (FM) modeling software (Kernkamp et al., 2011; Reyns et al., 2025) is applied to study the hydrodynamics, sediment transport and morphological development at the selected site. The recently developed Delft3D FM model is the successor of the Delft3D software. Delft3D has been widely used in sand wave research to simulate among others the growth of sand waves from small perturbations (e.g., Borsje et al., 2014; Van Gerwen et al., 2018) and the migration of fully grown sand waves (e.g., Krabbendam et al., 2021; Leenders et al., 2021). Key advantages of Delft3D FM include the use of unstructured meshes (flexible meshes) and the capability to run parallel simulations across multiple computational nodes. These enhancements combined with more efficient coding structure significantly reduce computational time. The fundamental physical

21699011, 2026, 10, Downloaded from https://agupubs.onlinelibrary.wiley.com/doi/10.1029/2025JF008603 by Technical University Delft, Wiley Online Library on [14/10/2026]. See the Terms and Conditions (https://onlinelibrary.wiley.com/terms-and-conditions) on Wiley Online Library for rules of use; OA articles are governed by the applicable Creative Commons License

21699011, 2026, 10, Downloaded from https://agupubs.onlinelibrary.wiley.com/doi/10.1029/2025JF008603 by Technical University Delft, Wiley Online Library on [14/10/2026]. See the Terms and Conditions (https://onlinelibrary.wiley.com/terms-and-conditions) on Wiley Online Library for rules of use; OA articles are governed by the applicable Creative Commons License

principles, which are briefly outlined in the following sections, remain unchanged between the Delft3D 4 and Delft3D FM model. For further details, the user manual is referenced (Deltares, 2025). In this study the 2023.03 version of the software is applied.

2.2.1. Hydrodynamics

To simulate hydrodynamics, the Delft3D FM model uses the shallow water equations, comprising a continuity equation and momentum equations across three spatial dimensions. Given that the horizontal scales are much larger than the vertical one, the vertical momentum balance can be simplified to hydrostatic pressure. This system of equations is solved using a finite volume solver on a staggered grid, with explicit time integration (except for water levels). This necessitates a Courant limitation based on flow velocities for the time-step, which is applied automatically according to a user-defined Courant number. The basic equations are included in Supporting Information S1.

2.2.2. Sediment Transport and Morphology

The L. C. Van Rijn (2007) sediment transport equations are applied to calculate the bed load transport generated by near bed currents, following Overes et al. (2025). Since the study site is bed load dominated, suspended sediment transport is excluded from the simulations. This reasoning is supported by the local Rouse number, which is even with the strongest tidal currents above the limit of 2.5 for incipient suspended sediment transport (Fredsoe & Deigaard, 1992), with a value between 2.6 and 6.4 for spring and neap tide respectively. The (uncorrected) bed load transport is calculated using the following equation:

$$S_b'' = 0.5\rho_s d_{50} D_*^{-0.3} \left(\frac{\tau'_{b,c,t}}{\rho_w}\right)^{0.5} T'(t) \tag{1}$$

where ρ_s and ρ_w are the density of the soil and water, set at 2,650 and 1,025 kg/m^3 respectively, d_{50} denotes the median sediment size and D_* is the dimensionless grain diameter (see (L. C. Van Rijn, 2007)). $\tau'_{b,c,t}$ is the instantaneous grain-related bed-shear stress due to currents and $T'(t)$ is the instantaneous dimensionless excess shear parameter. The underlying equations are included in Supporting Information S1. The effect of bed slope on the threshold for sediment transport is already included in this formulation. The longitudinal (in flow direction) and transverse (perpendicular to flow direction) gravitational bed slope effects on sediment transport magnitude and direction are included separately using the formulations by Bagnold (1966) and Ikeda (1982) respectively. First the calculated bed load transport rate is adjusted for longitudinal bed slope effects, by scaling the transport rate with a factor α_s while retaining the transport direction:

$$\vec{S}_b' = \alpha_s \vec{S}''_b \tag{2}$$

$$\alpha_s = 1 + \alpha_{bs}\left(\frac{\tan(\phi)}{\cos\left(\tan^{-1}\left(\frac{\partial z}{\partial s}\right)\right)\left(\tan(\phi) + \frac{\partial z}{\partial s}\right)} - 1\right) \tag{3}$$

where ϕ is the angle of repose for the sediment, set at 30°, and $\frac{\partial z}{\partial s}$ is the bed slope in the direction of sediment transport (s). α_{bs} is a user-defined scaling parameter which adjusts the dominance of longitudinal bed slope effects. It is set at its default value of 1, following Overes et al. (2025), reducing the formulation to the original equation derived by (Bagnold, 1966).

Subsequently the transverse (perpendicular to flow direction) slope effects are included by calculating an additional sediment transport rate, which is acting in a direction (n) perpendicular to the original transport direction (s). In this way both the magnitude and direction of the sediment transport are affected. This perpendicular transport rate ($S_{b,n}$) is calculated using the transport rate scaled for longitudinal (in flow direction) bed slope effects:

$$S_{b,n} = |S_b'|\alpha_{bn}\frac{u_{b,cr}}{|\vec{u}_b|}\frac{\partial z_b}{\partial n} \quad (4)$$

where $u_{b,cr}$ is the critical near-bed fluid velocity and u_b is the simulated near-bed fluid velocity. Moreover, $\frac{\partial z_b}{\partial n}$ is the bed slope in the direction perpendicular to the original sediment transport direction. Here also a user-defined scaling factor is included, namely α_{bn}, which has a default value of 1.5. Sand wave slopes are generally not steep enough to cause avalanching or purely slope-induced creep. This is also the case for the sand waves and trench slopes in our case. These processes are not included in the simulations. Creep of sediment (i.e., transport below the threshold of motion) is included in the L. C. Van Rijn, 2007 sediment transport formulation (see L. Van Rijn (2006)), but is not directly related to the slope steepness.

After transforming the transport rates from the coordinate system based on the local transport direction to the x,y grid, the bed evolution can be calculated. This is done using the Exner continuity equation:

$$(1-\varepsilon_p)\frac{\partial z_b}{\partial t} + \frac{\partial S_{b,x}}{\partial x} + \frac{\partial S_{b,y}}{\partial y} = 0 \quad (5)$$

where ε_p represents the bed porosity, assumed to be 0.4, and $\frac{\partial z_b}{\partial t}$ is the rate of change of bed level over time.

2.3. Sand Wave Model Set-Up

2.3.1. Computational Mesh and Bathymetry

At the location where the trench crosses the two sand waves, shown in Figure 1, a numerical model is created. To allow for a fine resolution near the trench, while keeping the boundaries of the model at sufficient distance, an unstructured mesh is used. This significantly reduces the number of horizontal cells in the numerical grid. The grid consists of several patches of rectangular cells, which double in size in both directions at each transition and are connected using a band of triangular cells. The orientation of the rectangular cells is aligned with the direction of the trench. This also ensures a good alignment with the local currents, since the main tidal axis is directed approximately along the trench. The finest grid resolution is applied in and around the trench over a width of 100 m, where the steepest slopes in the cross-trench dimension are found. There the grid has a size of 2 m in the along trench direction and 2.5 m in the cross trench direction. Further away from the trench the grid size in the cross trench direction is 5 m for a patch of 100 m on both sides, while the along trench grid size remains 2 m. Outside this area both grid sizes double to arrive at 10×4 m cells in the area further away from the trench. These increased grid sizes in the cross trench direction are implemented since bathymetric changes in this direction, along the sand wave crest, are limited further away from the trench. In the along trench direction the sand waves still cause significant bathymetric changes, thereby limiting the acceptable grid size in this direction. Outside of the morphological model domain the grid sizes increase up to a maximum grid size of 128 by 320 m. A more detailed description of the grid layout and a visual overview are included in Supporting Information S1. The vertical grid consists of 30 sigma layers with increasing thickness from 0.1% of the waterdepth close to the bed, to 16.2% near the surface. In between the layers grow exponentially with a factor 1.19.

The available bathymetric surveys are used to create the initial model bathymetry. Since the 2018-out survey only covers an area with a width of 80 m surrounding the trench, this survey is combined with the slightly wider 2018-in survey and the 2016 survey. This combined bathymetry is shown in Figure 1. Subsequently the superimposed megaripples are filtered from the combined measurements since the numerical grid is too coarse to resolve these bedforms. If included these would quickly smoothen out and thereby distract from the sand wave processes which are the subject of this study. The bed roughness for hydrodynamic calculations is increased with respect to smooth bed to compensate for the exclusion of these bedforms. For this a highpass fourier filter is applied with an ellipsoidal kernel, which has a wavelength of 30 m in the direction of 50°N, approximately perpendicular to the megaripple crests. The minor axis of the ellipsoid has a wavelength of 10 m, to account for slight directional variations of the megaripples. This filtering does not significantly affect the sand waves, which have a wavelength of 200–300 m. Lowering of the sand wave crest height due to the filter application was found to be around 0.1–0.3 m, of which part can be attributed to megaripple presence. The sand waves are included with their full height in the area of interest. Outside of this area the sand waves dampen to arrive at the large scale bathymetry

21699011, 2026, 10, Downloaded from https://agupubs.onlinelibrary.wiley.com/doi/10.1029/2025JF008603 by Technical University Delft, Wiley Online Library on [14/10/2026]. See the Terms and Conditions (https://onlinelibrary.wiley.com/terms-and-conditions) on Wiley Online Library for rules of use; OA articles are governed by the applicable Creative Commons License

21699011, 2026, 10, Downloaded from https://agupubs.onlinelibrary.wiley.com/doi/10.1029/2025JF008603 by Technical University Delft, Wiley Online Library on [14/10/2026]. See the Terms and Conditions (https://onlinelibrary.wiley.com/terms-and-conditions) on Wiley Online Library for rules of use; OA articles are governed by the applicable Creative Commons License

from the DCSM in the domain with larger cell sizes. There the grid sizes are too large to resolve the individual sand waves. This combined bathymetry is interpolated to the grid cell centers to create the initial bathymetry for the simulations. For two model cases and adapted bathymetry is applied to mimic different trench designs. The creation of these bathymetries is explained in Supporting Information S1.

2.3.2. Hydrodynamic Forcing Conditions

To simulate the hydrodynamics over the period between the measurements, the model is (offline) coupled to the large-scale DCSM (Deltares, 2018). This is done at the four open boundaries of the local model, where advection velocity boundary conditions are applied. These boundary conditions impose a waterlevel as well as the incoming momentum advection as a profile over depth at inflow boundaries. At outflow boundaries the boundary condition automatically changes to a Neumann type boundary condition. The waterlevels and current velocities (used for the incoming momentum advection) are extracted from a DCSM run for the considered period. These hydrodynamics include both tidal and non-tidal, for example, meteorological, forcing, see Deltares (2018). Validation shows that in this way the hydrodynamics are transferred well between the models, with a RMSE of 0.008 m for the waterlevels and a RMSE of 0.027 m/s for both the velocities in W-E and S-N direction for the first 365 days of the simulation. The comparison is included in Supporting Information S1. Although the DCSM does impose a wind at the water surface, this wind forcing is not included in the local model, since its effects on the hydrodynamics were found to be negligible due to the limited size of the domain. However, the currents created by this wind in the DCSM are transferred through the lateral hydrodynamic boundaries. Waves are excluded from the model, both for simplicity and to reduce computational effort, since their effect on the morphological development is assumed to be negligible due to the significant water depth of around 30 m. This is supported by a calculation of the shear-stress under representative wave conditions, showing only marginal increase in shear stress when added to an average peak tidal current (see Bloem (2024)).

2.3.3. Model Settings

The vertical turbulent eddy viscosity is calculated using the k-epsilon turbulence model, based on Borsje et al. (2013). A background horizontal eddy viscosity of 0.1 $m^2\ s^{-1}$ is assumed. Bed roughness for hydrodynamic calculations is represented by a Chézy roughness coefficient of 70 $m^{1/2}/s$. This roughness is based on presence of ripples and megaripples. The roughness height is calculated using the L. Van Rijn (1993) bedform roughness formulations, assuming a ripple length of 17 cm as observed in Damveld et al. (2018) combined with height of 1.7 cm (based on a steepness (H/L) of current ripples of 0.1 following L. Van Rijn (1993)) and megaripples with a length of 15 m and a height of 0.2 m, based on in situ observations. These bed roughness values are subject to some uncertainty. However, the influence of bed roughness for hydrodynamics on the morphological results, when within reasonable limits, was found to be limited. The sediment transport calculations only include grain roughness for calculating bed shear stress, see Supporting Information S1. The maximum flow Courant number, which governs the timestep, is set to 0.9. A uniform sediment size is assumed, consisting of a single fraction with a log-uniform distribution. A median grain size, d_{n50}, of 350 μm is selected based on Verfaillie et al. (2006). No morphological scaling is applied (i.e., a morphological scale factor of 1), following (Overes et al., 2024), meaning that in these non-upscaled simulations, both hydro- and morpho-dynamics are computed using the same timescales. The bed slope parameters, which determine the dominance of gravitational bed slope effects for the sediment transport magnitude and direction (see Section 2.2.2), are set to their default values following Overes et al. (2025). For the applied formulations this means using a longitudinal (in flow direction) bed slope parameter (α_{bs}) of 1 and a transverse (perpendicular to flow direction) bed slope parameter (α_{bn}) of 1.5. An overview of the main model parameter settings is provided in Table 1.

2.3.4. Computational Setup

The simulations are run on the Snellius super computer, where one node with 128 cores is utilized. The model domain is divided into 128 partitions, which are run in parallel. Due to the time limit for the use of these nodes, the model is restarted every 5 days using model generated restart files. Over these 5 days a period of approximately 147 days can be simulated. At the start of the runs a morphostatic spin-up of two tidal cycles is included.

21699011, 2026, 10, Downloaded from https://agupubs.onlinelibrary.wiley.com/doi/10.1029/2025JF008603 by Technical University Delft, Wiley Online Library on [14/10/2026]. See the Terms and Conditions (https://onlinelibrary.wiley.com/terms-and-conditions) on Wiley Online Library for rules of use; OA articles are governed by the applicable Creative Commons License

Table 1
Overview of Parameter Settings

Parameter	Symbol	Value	Unit
Chézy roughness coefficient	C	70	$m^{1/2}/s$
Horizontal eddy viscosity	ν_H	0.1	m^2s^{-1}
Maximum Courant number	–	0.9	–
Median sediment grain size	$d_{n,50}$	350	μm
Longitudinal bed slope parameter	α_{bs}	1	–
Lateral bed slope parameter	α_{bn}	1.5	–
Morfac	–	1	–

2.4. Model Cases

To study the hydrodynamics, sediment transport and morphology of the sand wave trench system, five simulation cases are designed. The base case (Base) captures the long-term development of the trench after dredging. By comparing the morphodynamic results from this case to measured morphodynamics, we can build trust in the simulations. Additionally, it is used to investigate how the trench infill patterns change over time. The start and end dates match the dates of the available measurement surveys and the initial bathymetry is based on (a combination of) these surveys (see Section 2.3.1). The hydrodynamic forcing is based on a DCSM run for this same period and thereby matches the real conditions in the field, including non-tidal effects such as storms.

Additionally, four short-term runs are created to investigate different 3D processes in and around the trench and to test the effects of different trench designs. Firstly, the impact of the dredging on the 3D current structure and sediment transport patterns is investigated using a short-term run with hydrodynamics based on calm conditions (Calm). The initial bathymetry for this short-term simulation is extracted from the Base simulations after 100 days. This is done to limit the effects of initial numerical adaptation of the sand wave bathymetry (see Overes et al. (2025) and Section 2.6) and to ensure the sand waves are recovering (i.e., they have passed the adaption period found by Larsen et al. (2020)). Secondly, to study the impact of storm-induced currents a new case (Storm) is created based on the Calm case, but with different hydrodynamic forcing from the period when storm Ciara passed the area. The results of this run are compared to the Calm case to discern the effects of storm-induced currents. Lastly, two different trench designs are tested, which are adaptations of the real trench in the Base case, based on the (combined) 2018-out measurements. In Wide the bottom of the trench is widened with a factor 2 (40 m instead of 20 m), but the slopes and surrounding sand waves remain the same. In case Gentle the slopes (and surrounding bathymetry) are widened (made more gentle in cross-trench direction) with a factor 2, while the bottom of the trench retains the same width (20 m). Except for the trench bathymetry the model set-up of these two cases is the same as the Base run, allowing for inter comparison. The cases are summarized in Table 2.

2.5. Calculating Transverse Sediment Balance

To assess how much infilling of the trench occurs, and where exactly this sediment ends up, we investigate the transverse sediment balance (in the cross trench direction). This is done through summation of the volume changes in along trench direction. This volume summation makes it easier to visualize and analyze the 3D simulation results. Moreover, migration of the sand waves is filtered out of the sedimentation erosion patterns,

Table 2
Overview of Simulation Cases

Name	Duration	Period hydrodynamics	Initial bathymetry
Base	3.2 years	9 April 2018–28 June 2021	2018-out meas. (combined)
Calm	10 days	24 October–3 November 2019	Base model after 100 days
Storm	5 days	7–12 February 2020	Base model after 100 days
Wide	145 days	9 April–6 September 2018	Adapted 2018-out meas. (combined)
Gentle	145 days	9 April–6 September 2018	Adapted 2018-out meas. (combined)

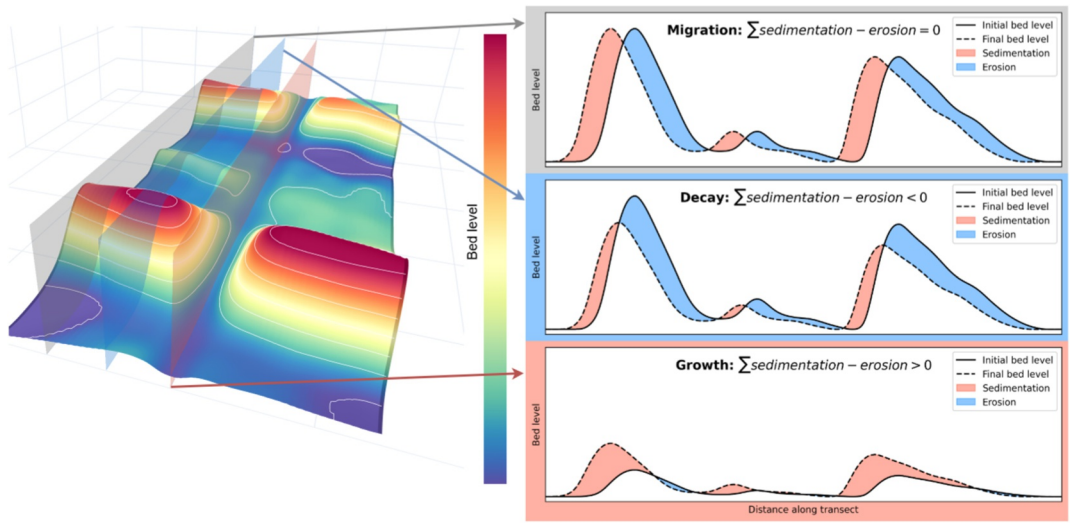


Figure 2. Example of transverse sediment balance calculation: volume change summation over along trench planes. Figures on the right illustrate the outcome of this summation for different cases.

since this is essentially a redistribution of sediment over the direction perpendicular to the sand wave crests (along the trench) (Figure 2). This reasoning also applies to the slight reshaping of the sand waves which manifests as a rounding of the crests in the numerical model, see for example, Krabbendam et al. (2021) and Overes et al. (2025). This reshaping is also observed in the long-term morphological results of this study (see Section 2.6).

To arrive at the transverse volume changes, transects are defined at each row of cells. Up to 50 m from the trench center (total 100 m width), these transects have a spacing of 2.5 m. Outside of this area the spacing grows with the increased cell size to 5 m. In the along transect direction the cell size is always 2 m and with an equal length of 580 m spanning the detailed sand wave domain, each transect consists of the same amount of cells (290). The bed level differences over a certain time span are summed along the transect and multiplied with the along trench cell size (2 m) to arrive at the volume change per running meter (in the cross trench dimension). These same transects are applied to the measurements to validate the transverse sediment budget (see Figure 4).

2.6. Model Comparison to Measurements

To build trust in the morphodynamic simulations, the results of the Base case are compared to the measured morphodynamics. If we consider the spatial sedimentation-erosion patterns, we see that the overall patterns are reproduced well in the Base model (Figure 3). The highest sedimentation rates are found in the trench at the location between the two surrounding crests, where the sand waves are regrowing. Compared to the measurements the sedimentation in the simulation is more diffused, leading to a broader (less pointy) and significantly lower crests than found in the measurements, with a crest height difference of 1.5–2.5 m. The troughs of the sand waves do not erode, keeping these levels at the dredged trench level in both the measurements and the simulation This shows that the model has difficulty reproducing the very pointy crests found in reality. The recovering sand waves in the simulation have more rounded, broader crests. The highest erosion rates are found at the location of the sand wave crests right next to the trench. These crests decrease in height and thereby feed sediment into the trench. On the south western side of the crests sedimentation is observed, indicating migration of the sand waves toward the ebb direction (south west) in both the simulation and observations. Possibly this sedimentation is increased slightly in the model due to reduction of the slope steepness following the initial shape adaptation in the simulation.

To assess the ability of the simulation to reproduce the observed infilling of the trench the transverse sediment balance (see Section 2.5) is calculated for the long-term Base model case and the resulting average bed level changes are compared to those from the measurements (2018-out and 2021, excluding megaripples). Through summation of the sedimentation- and erosion volumes over the along trench dimension the migration of the sand waves as well as the slight shape adaptation of the modeled sand waves is filtered out. When comparing the

21699011, 2026, 10, Downloaded from https://agupubs.onlinelibrary.wiley.com/doi/10.1029/2025JF008603 by Technical University Delft, Wiley Online Library on [14/10/2026]. See the Terms and Conditions (https://onlinelibrary.wiley.com/terms-and-conditions) on Wiley Online Library for rules of use; OA articles are governed by the applicable Creative Commons License

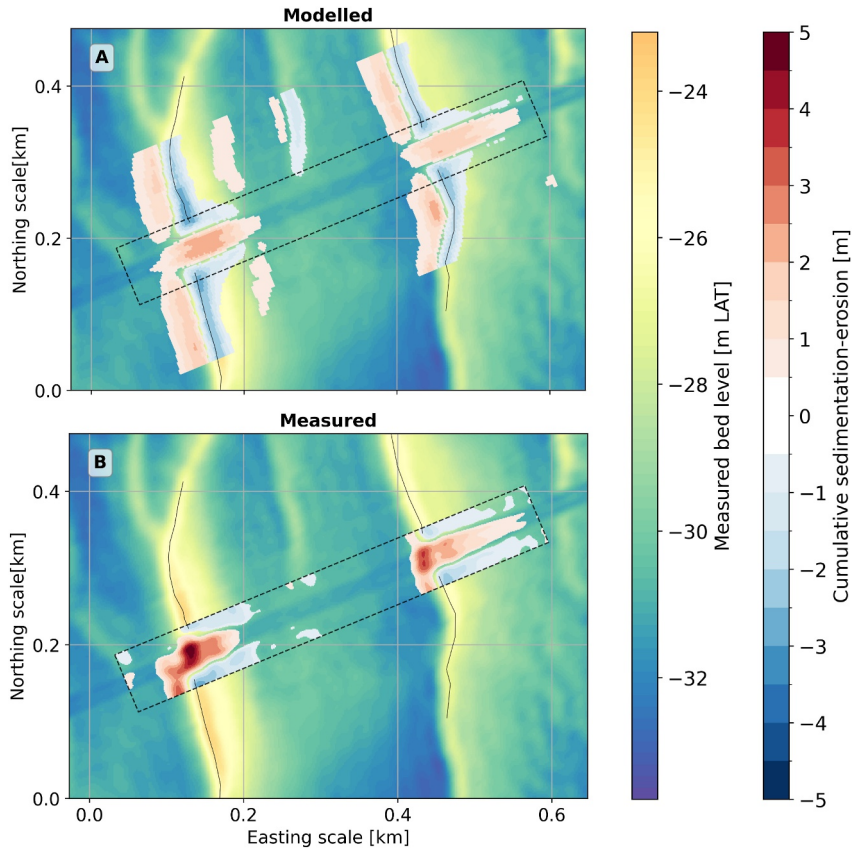


Figure 3. Bed level change over the full period between measurements (April 2018–July 2021): (a) from case Post model and (b) from measurements (excluding megaripples, extent limited by width of 2018-out survey). Red tones indicate bed heightening (sedimentation), blue tones indicate bed lowering (erosion). Black lines indicate the location of the sand wave crests in the initial bathymetry.

average along trench bed level changes over the trench, very similar sedimentation-erosion patterns are observed between the model and the measurements (Figure 4). Compared to the measurements, the simulation slightly underestimates the along-trench averaged sedimentation and erosion rates. The highest sedimentation rates are found surrounding the trench center. The measurements show maximum along-trench averaged bed heightening of around 1 m, where in the simulation this averaged heightening is 0.8 m. Both the model simulation and the measurements show a slightly higher sedimentation rate right next to the trench center. This pattern is the result of the transition from a flat trench bed right after dredging to a more rounded trench, with the deepest point exactly at the center. The transition from a (on average) sedimentary to an erosional trend is found around 15–20 m to the north and south from the trench center. The location of this transition is reproduced well in the simulation. Further to the north and south the along-trench averaged bed level has decreased, indicating erosion of the surrounding sand waves in both the measurements and the simulation. The erosion is slightly underestimated in the simulation. Since the survey after dredging only covers the 80 m surrounding the trench center, no comparison could be made beyond this scope. The total volume change within this area is just over 5,000 m^3 (about 1/3 of the trench infill volume) in both measurements and the model. This sediment deficit indicates that part of the infilling volume does not originate from the trench slopes and sand waves directly surrounding the trench, but has its origin at a distance of over 40 m. Alternatively part of the sediment could originate from along the trench direction, however sediment transport over these boundaries is limited in the model results.

Since there is no further incision of the troughs below trench level (the sand waves thus regrow on top of the trench level), the mismatch in regrowing sand wave height is the result of a difference in shape of the regrowing sand wave, rather than of a mismatch in the volume regrowth. Such shape mismatches can be caused by slight mismatches in diffusive process strength, which accumulates over time in morphological models. These shape

21699011, 2026, 10, Downloaded from https://agupubs.onlinelibrary.wiley.com/doi/10.1029/2025JF008603 by Technical University Delft, Wiley Online Library on [14/10/2026]. See the Terms and Conditions (https://onlinelibrary.wiley.com/terms-and-conditions) on Wiley Online Library for rules of use; OA articles are governed by the applicable Creative Commons License

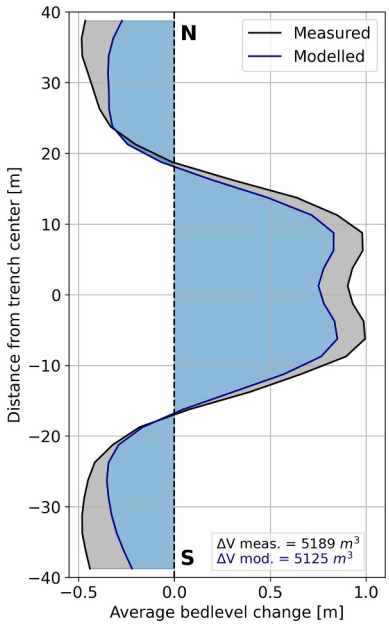


Figure 4. Bed level change averaged over the along trench direction for the full period between measurements (April 2018–July 2021) compared between Base case simulation and measurements (excluding megaripples). Limited to the width of the 2018-out measurements (80 m). ΔV indicates the volume change over the full area for the measurements (meas.) and model (mod.).

mismatches have been observed before (see e.g., Krabbendam et al., 2021; Overes et al., 2025) and are most prominent for steep and pointy sand waves, alike the sand waves in this study. The reason for the shape adaptation is still unresolved, but could be due to (a combination of) slight inaccuracies in the hydrodynamics (e.g., due to the exclusion of non-hydrostatic effects) or sediment transport representations (e.g., due to excluded sediment heterogeneity), which stack over time in a morphodynamic model. These shape adaptations are observed in 2DV models and thus likely a result of sediment diffusion in the direction perpendicular to the crest. Therefore, it is deemed unlikely that these inaccuracies significantly influence the sediment balance in the trench transverse direction. Since the regeneration volumes are well reproduced in the model, these will be used for further analysis.

3. Results

Now that we have built trust in the morphodynamic model results we move on to studying 3D processes leading to trench infill an sand wave volume regrowth. Firstly, the hydrodynamic and sediment transport patterns in and around the trench are analyzed for a calm period through a short-term simulation (Calm). Secondly, the impact of a storm on the trench infill is analyzed by comparing two simulations with different forcing conditions, but otherwise identical setup (Calm and Storm). Thirdly, the multiyear morphological development of the trench is analyzed using the long-term run (Base), by investigating the transverse sediment balance. Lastly, two different trench designs are applied and analyzed using the Wide and Gentle cases.

3.1. Tide-Averaged Circulation Cells

Sand wave growth is closely linked to the vertical structure of the flow, which forms so called tide-averaged, vertical circulation cells (Hulscher, 1996). In these circulation cells the tide-averaged near-bed currents are directed from the trough toward the crest of the sand wave, thereby driving net bed load transport up the slope and inducing sand wave growth. To analyze the impact of the trench on this vertical flow structure we compare the results from the Calm case along the trench centerline to those along a transect 60 m South of the trench. This is outside of the region where erosion has taken place (around 40 m from trench center), due to adaptation of the trench side-slopes. Since residual currents can make it more difficult to visualize and quantify the strength of the vertical circulation patterns, we have chosen a period of exactly 6 tidal cycles over which the non-tidal currents are limited in strength and the average non-tidal current is close to zero. However, the non-tidal effects are still present in the model over this period, they are not filtered out. When stronger time-averaged residual currents are present, similar current variations over the vertical can be found relative to the time-averaged, depth-averaged residual current. This means that when compensated for the time-averaged, depth averaged residual current similar patterns will occur. In this case absolute current reversal may no longer be found, although the currents may locally be dampened significantly. Since morphology is affected by relative differences in sediment transport, this skewed current circulation can still induce sand wave growth. The averaged currents clearly show these circulation cells 60 m South of the trench, see Figure 5a. Overall the tide-averaged currents are ebb-dominated, as was expected due to the local tidal asymmetry. However, at the steep slopes of the sand waves, which face the flood current, the flood currents are dominant in the cells closest to the bed. This reversal of the tide-averaged near-bed currents drives the growth of the sand waves by causing net sediment transport to be directed toward the crest, where the currents converge, from both sides of the sand wave. Since the sand wave height from measurements was quite stable before trench installation, this up-slope circulation driven net sediment transport is compensated for by down-slope bed slope driven transport.

Next we focus on the currents inside the trench, to see how these were affected by the dredging. Along the transect exactly in the middle of the trench the tide-averaged circulation cells are still visible, although weakened (Figure 5b). The strongest tide-averaged horizontal current in flood direction is approximately 65% less compared to the transect 60 m South of the trench. The location where the near-bed, tide-averaged currents converge (around 100 and 440 m) are the same as next to the trench. The bed level along the trench center already shows slight

21699011, 2026, 10, Downloaded from https://agupubs.onlinelibrary.wiley.com/doi/10.1029/2025JF008603 by Technical University Delft, Wiley Online Library on [14/10/2026]. See the Terms and Conditions (https://onlinelibrary.wiley.com/terms-and-conditions) on Wiley Online Library for rules of use; OA articles are governed by the applicable Creative Commons License

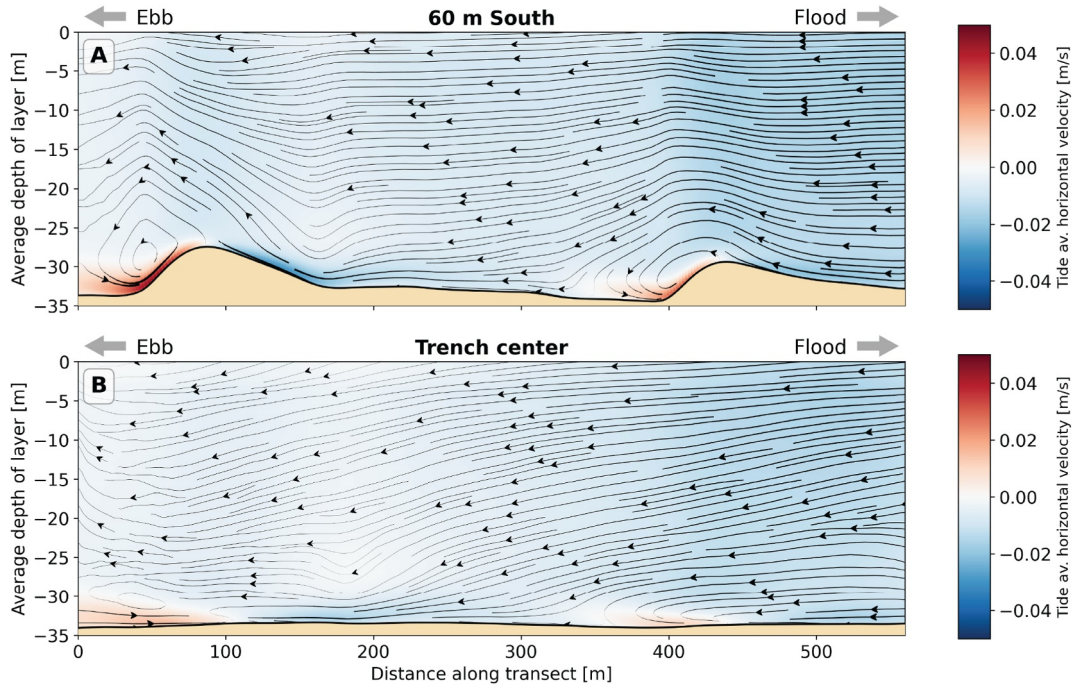


Figure 5. Tide-averaged, vertical current circulation for case Calm, at 60 m South of the trench (a) and along the trench centerline (b). Colors indicate horizontal current strength, positive is flood directed.

undulations at the former locations of the sand waves, with an amplitude of around 0.25 m. To investigate the influence of these remaining undulations an additional simulation was set up in which the trench was flattened over a width of 5 cells (12.5 m) in the center of the trench. The results of this simulation show that removing these bed undulations reduces the strength of the circulation cells by only 5%. These results are included in Supporting Information S1. The circulation cells within the trench (Figure 5b) are thus mostly not locally generated, but occur under the influence of the circulation cells which are still present at (close to) full strength on both sides of the trench, where the sand waves are not dredged. In this case the sediment transport due to the tide-averaged circulation is not compensated for by bed slope-induced transport, due to the limited slope steepness, and the circulation thus drives sand wave growth.

3.2. Horizontal Patterns in Hydrodynamics and Sediment Transport

Next we analyze the horizontal pattern of current velocities and sediment transport after dredging to provide insight into the sideways infilling of the trench, using the Calm case. This analysis is done for the same calm, tide dominated period of 6 tidal cycles as the above vertical transect analysis of the 3D simulation. Since the system is bed load-dominated, especially the near-bed velocities are leading for morphological development. Therefore we have extracted the near-bed velocities used for the sediment transport calculations (also called the characteristic velocity). Since the depth of the near-bed velocity output changes over time and space due to the stretching and compression of the sigma layers, the velocities cannot directly be averaged over time. The velocity changes significantly with depth and therefore output at a higher level above the bed (with flood water levels) would result in a higher velocity (therefore leading to flood dominance). Therefore, the velocity is interpolated based on a log scale from the output depth to an imaginary depth-averaged velocity, which we call the representative near-bed velocity, to ensure unbiased comparison between the velocities extracted at different output depths. This interpolation is done in exactly the same way as applied in the bed load calculations of the model, see Supporting Information S1 and L. Van Rijn et al. (2004). The tide-average of these velocities is shown in Figures 6a and 6b and shows that over the whole area the tide-averaged near-bed velocity is generally directed up-slope, also at the sides of the trench. This is caused by shadowing of the slope for down-slope directed currents and exposure of the slope to currents accelerating up-slope. At the crests of the sand waves and at the former crest location within the trench, minima in the average near-bed velocity are found due to the convergence of the tide-averaged vertical

21699011, 2026, 10, Downloaded from https://agupubs.onlinelibrary.wiley.com/doi/10.1029/2025JF008603 by Technical University Delft, Wiley Online Library on [14/10/2026]. See the Terms and Conditions (https://onlinelibrary.wiley.com/terms-and-conditions) on Wiley Online Library for rules of use; OA articles are governed by the applicable Creative Commons License

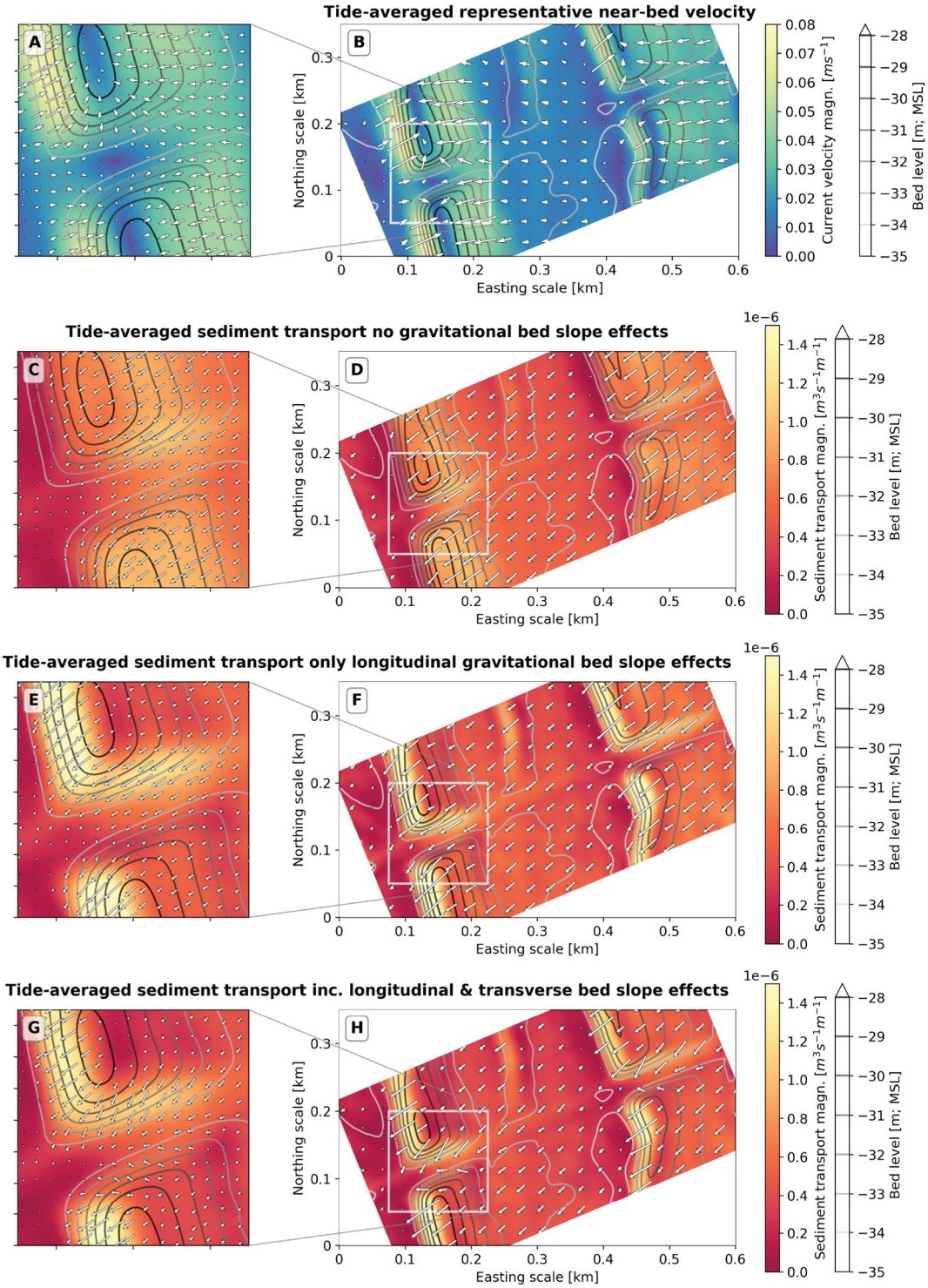


Figure 6. (a and b) Tide-averaged representative near-bed velocity, a representative, imaginary depth-averaged velocity logarithmically upscaled from near-bed to allow for accurate time-averaging (see Supporting Information S1), (c and d) Tide-averaged bed load sediment transport without gravitational bed slope effects, (e and f) Tide-averaged bed load sediment transport with only longitudinal bed slope effects (see Equation 3), (g and h) Tide-averaged bed load sediment transport with bed slope effects.

21699011, 2026, 10, Downloaded from https://agupubs.onlinelibrary.wiley.com/doi/10.1029/2025JF008603 by Technical University Delft, Wiley Online Library on [14/10/2026]. See the Terms and Conditions (https://onlinelibrary.wiley.com/terms-and-conditions) on Wiley Online Library for rules of use; OA articles are governed by the applicable Creative Commons License

21699011, 2026, 10, Downloaded from https://agupubs.onlinelibrary.wiley.com/doi/10.1029/2025JF008603 by Technical University Delft, Wiley Online Library on [14/10/2026]. See the Terms and Conditions (https://onlinelibrary.wiley.com/terms-and-conditions) on Wiley Online Library for rules of use; OA articles are governed by the applicable Creative Commons License

circulation cells. The strength of this current circulation gradually reduces toward the trench due to the reducing height and steepness of the sand waves. Although the non-linear dependency of sediment transport on current velocity is not taken into account in this tide-averaging (the contribution of high velocities is underestimated), it is unlikely that the near-bed currents directly contribute to the infilling of the trench in absence of gravitational bed slope related effects. This is confirmed by removing (most of) the bed slope effects from the sediment transport calculations, which is done in Figures 6c and 6d. In this run the gravitational bed slope effects are switched off and only the effect of bed slope on threshold for sediment transport remains (which could not be removed). In this case the sediment transport is directed toward ebb, although the transport almost seizes to exist close to steep slopes of the sand waves due to shadowing of the currents. The sediment transport is directed along the trench and thus barely contributes to trench infill in the absence of gravitational bed slope effects, which is corroborated when looking at the sedimentation-erosion patterns, see Supporting Information S1.

If we start adding the gravitational bed slope effects, we see significant changes in sediment transport magnitude and direction. Especially the longitudinal (in flow direction) bed slope effects are important for the transport magnitudes, increasing the tide-averaged transport by a factor 5–10 on the steep slopes of the sand waves (with the default α_{bs} value of 1), see Figures 6e and 6f. The transverse (perpendicular to flow direction) bed slope effects, on the other hand, are responsible for directing sediment transport into the trench along the trench side slopes, while their effect on transport magnitudes is limited (with the default α_{bn} value of 1.5), see Figures 6g and 6h. Thereby this process is likely most important for trench infill with this specific orientation. When considering bed slope effects, the largest tide-averaged sediment transport magnitudes are found at the steepest trench slopes, next to the sand wave crests, and the south-west facing steep sand wave slopes. At both of these locations the down-slope directed sediment transport is opposing the up-slope directed tide-averaged near-bed velocities. At the steep trench slopes, next to the surrounding sand wave crests, sediment is transported from the surrounding sand wave crests into the trench. Over time, this transport causes lowering of the surrounding crests and volume regrowth of the sand wave crest in the trench. Further from the crests the sediment transport seems largely unaffected by the trench, thereby indicating limited trench infilling. The sediment transport magnitudes at the northern slope of the trench are significantly higher than those on the southern slope. This can be explained by the ebb dominance in the tidal signal, since the ebb tidal currents enter the trench from the north due to the slight inclination between the trench and the tidal axis.

3.3. Transverse Sediment Balance

To see how storm-induced currents influence the trench infilling we analyze the transverse sediment balance for two cases with different hydrodynamic forcing, but otherwise identical set-up. The calculation of the transverse sediment balance is explained in Section 2.5. First we consider the Calm case, in which the residual currents are relatively low and the hydrodynamics are tide dominated. We have chosen a period in which the tidal currents are similar to those during storm Ciara (a few days before spring tide) to allow for inter comparison. In this case we see alternating infilling from the north and south side during the ebb and flood current respectively, due to the slight angle between the trench and the main tidal axis (Figure 7a). During the ebb phase (negative current direction) sediment is eroded from the northern slope and deposited mainly in the northern part of the trench. On both slopes erosion is observed, but this erosion is slightly larger on the southern slope where the near bed velocities encounter the slope and accelerate. For the flood tidal phase this process is reversed. From the sedimentation and erosion rates it is clear that the strength of the tidal currents has a significant effect on the trench infill rates. The ebb tidal currents show a slight diurnal inequality, which clearly translates into the morphological changes.

3.3.1. Influence of Storm-Induced Currents

Next we assess the impact of storm induced currents using the Storm case through the transverse sediment balance (Figure 7b). The storm currents were aligned with the flood direction at the field location. During the peak of the storm the sedimentation-erosion pattern is similar to that observed in calm conditions. However the magnitude of the sedimentation and erosion is amplified significantly, by a factor of around 2.6 and 2.8 for the peak sedimentation and erosion respectively. This causes considerable sedimentation on the southern side of the trench bed and significant erosion of the northern slope. However, during both the preceding and following ebb phase, the tidal current are dampened by the storm, thereby suppressing the morphological changes and trench infill.

10.1029/2025JF008603

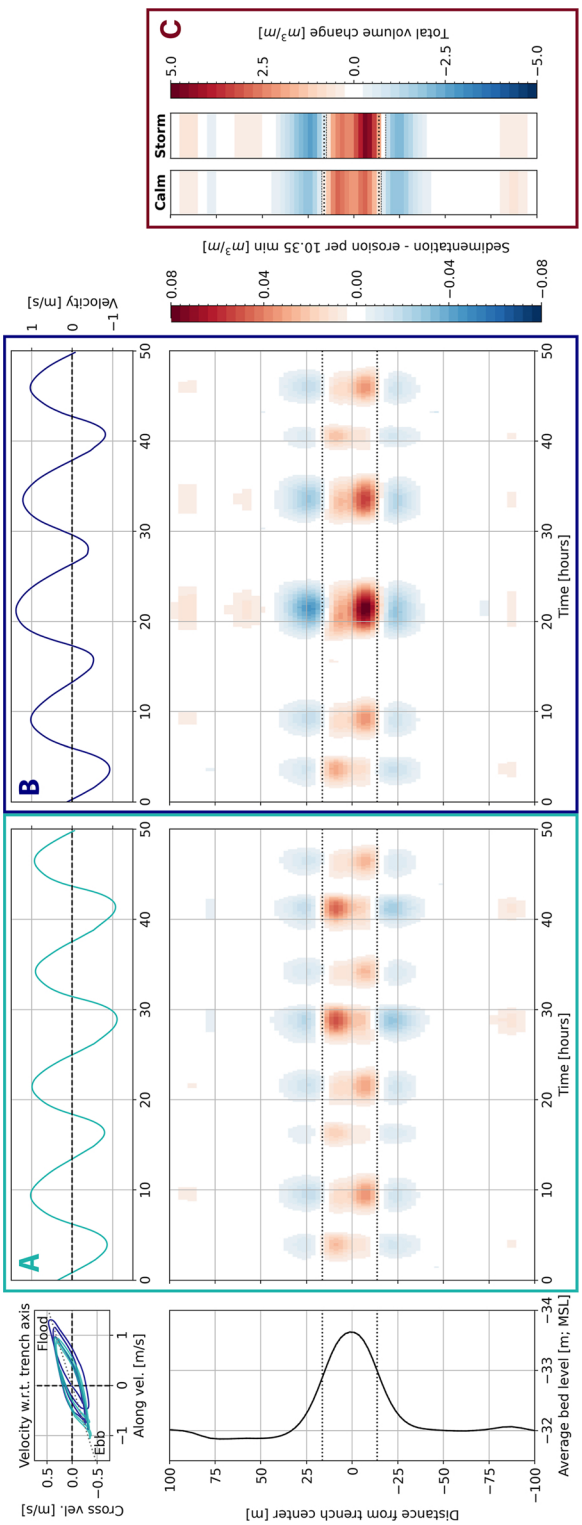


Figure 7. Timestack of along-trench averaged sedimentation and erosion (see Section 2.5) per tidal cycle over the cross trench direction for (a) calm conditions (Calm) and (b) during storm Ciara (Storm). Upper plots show total velocity magnitude, positive is flood directed. Left figure shows along-trench averaged bed levels, dotted horizontal lines indicate location of steepest slope. Upper left: velocity ellipse rotated with trench orientation. (c) Total transverse sediment balance over displayed 4 tidal cycles, for calm and storm conditions. Striped lines show extend of sedimentation area.

21699011, 2026, 10, Downloaded from https://agupubs.onlinelibrary.wiley.com/doi/10.1029/2025JF008603 by Technical University Delft, Wiley Online Library on [14/10/2026]. See the Terms and Conditions (https://onlinelibrary.wiley.com/terms-and-conditions) on Wiley Online Library for rules of use; OA articles are governed by the applicable Creative Commons License

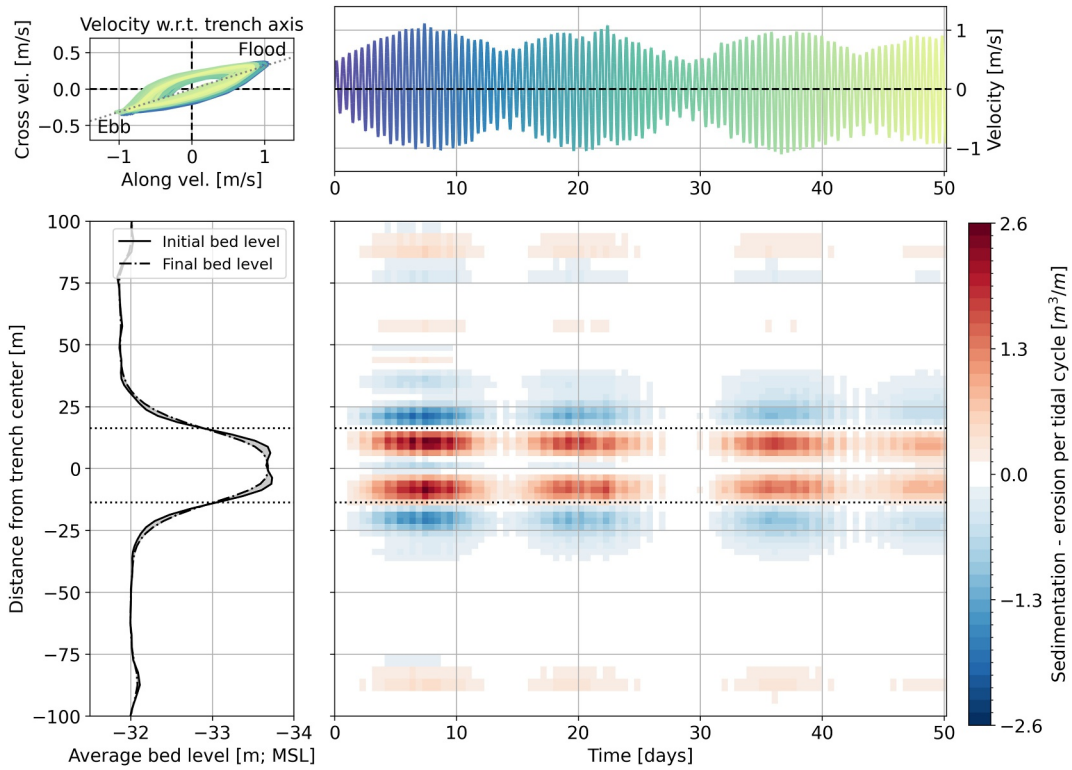


Figure 8. Timestack of along-trench averaged sedimentation and erosion (see Section 2.5) per tidal cycle over the cross trench direction for the first 50 days after dredging in the Base case. Including total velocity magnitude, positive is flood directed (upper), velocity ellipse rotated with trench orientation (upper left) and along-trench averaged bed levels (left). Dotted horizontal lines indicate location of steepest slope. Note difference in color scale with following figure.

When comparing the transverse sediment balance between the calm and stormy conditions, it is clear that the storm-induced currents had a significant impact on the sedimentation erosion pattern (Figure 7c). During the storm highly asymmetric infilling occurred, leading to an increased sedimentation volume in the southern half of the trench. At the same time the sedimentation of the northern side is decreased slightly. Overall the sedimentation volume at the location of the trench (between the striped lines in Figure 7c) has only increased by 25% over the 4 tidal cycles during the storm. For the storm event considered here, this shows that although the storm disrupts the symmetric infill pattern, its impact on total infill volume is limited. It should be noted that suspended sediment transport is excluded from the simulations and may increase temporarily under these extreme conditions, potentially increasing overall trench infill, although the observed asymmetrical patterns are likely unaffected.

3.3.2. Long Term Development

To study how the morphological changes impact the sedimentation erosion pattern we will extend the time horizon of our analysis, using the Base case. To this end we sum the sedimentation erosion over the tidal cycle instead of looking at intra-tidal dynamics. First we look at the initial response of the system in the 50 days after the dredging intervention. Right after the construction of the trench, sedimentation is only observed close to the trench slopes (Figure 8). At the center of the trench even some erosion is observed. Moreover, the spring-neap cycle is clearly distinguishable from the transverse sediment balance. During spring tide significant volumes are eroded from the trench slopes and deposited at the trench bed. During neap tide the changes in bathymetry are very limited. Next to this pattern also the diurnal inequality in the strength of the ebb current is distinguishable as a striped pattern in the transverse sediment balance. This is especially the case during neap tide, such as around day 42–43. At the end of the 50 day period the sedimentation patches on the north and south side have connected and there is no longer an (on average) erosive trend at the center of the trench. At this point in time the trench center is also the deepest point in the along-trench averaged bathymetry, where before the sides were slightly deeper. This can be seen from the average initial and final bed level in the leftmost plot in Figure 8.

21699011, 2026, 10, Downloaded from https://agupubs.onlinelibrary.wiley.com/doi/10.1029/2025JF008603 by Technical University Delft, Wiley Online Library on [14/10/2026]. See the Terms and Conditions (https://onlinelibrary.wiley.com/terms-and-conditions) on Wiley Online Library for rules of use; OA articles are governed by the applicable Creative Commons License

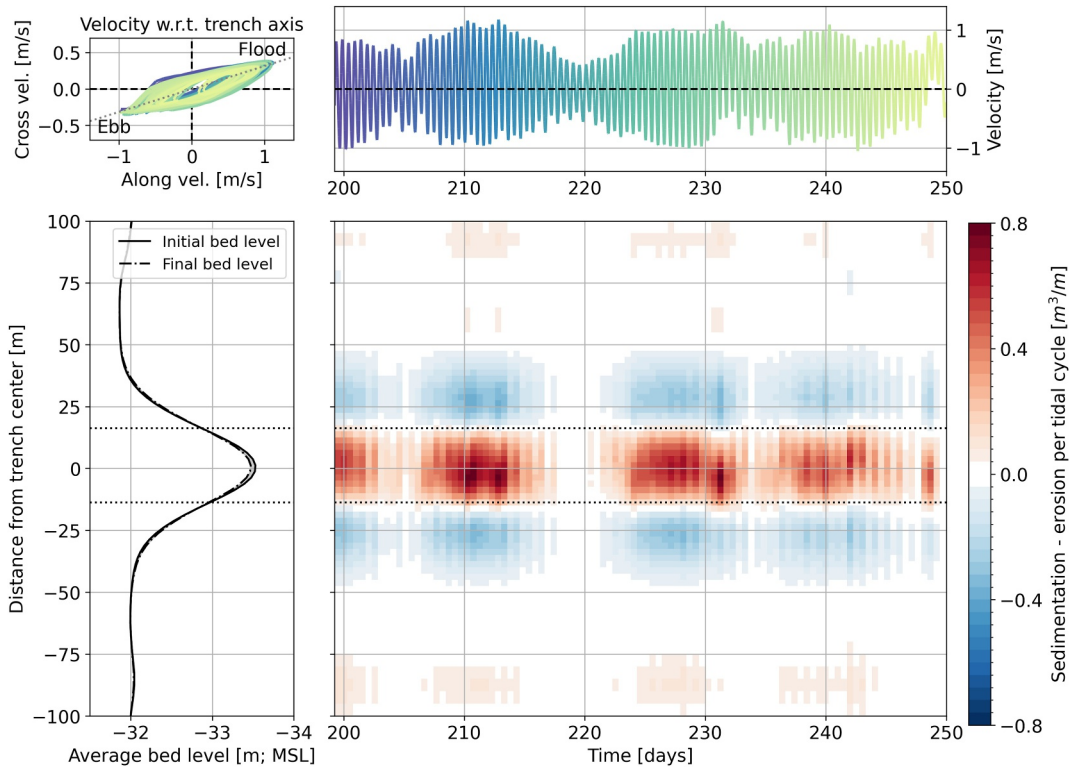


Figure 9. Timestack of along-trench averaged sedimentation and erosion (see Section 2.5) per tidal cycle over the cross trench direction for 200–250 days after dredging in the Base case. Including total velocity magnitude, positive is flood directed (upper), velocity ellipse rotated with trench orientation (upper left) and along-trench averaged bed levels (left). Dotted horizontal lines indicate location of steepest slope. Note difference in color scale with previous figure.

When we look at a later period within the Base case simulation, approximately a half year after the trench was dredged, we see that the system has changed drastically. The bathymetry of the trench (averaged over the along trench direction) has rounded further in the mean time and the average slope steepness of the trench sides has decreased significantly (Figure 9). The sedimentation around the center of the trench no longer consists of two separate areas to the north and south, but covers the full trench center. The location of this sedimentation patch moves with the asymmetry of the tide (more southwards in case of flood dominance and vice versa). The sedimentation and erosion volumes have decreased by around a factor 3 (note the difference in color scales). Lastly, the spring neap signal and the influence of the diurnal tidal signal are still clearly visible in the transverse sediment balance.

3.3.3. Impact of Trench Design

To investigate how the design of the trench influences the infill rate two additional model cases are set up in which the trench geometry is altered. This is done by stretching part of the bathymetry in the cross trench dimension with a factor 2 (see Supporting Information S1). In this way the case Wide, with a 2 times wider trench (40 m instead of 20 m) and case Gentle with 2 times gentler trench slopes (1:10 instead of 1:5) are created. Both cases are run for the first 145 days after dredging, to investigate the initial response of the system. In case a wider trench is created, the initial sedimentation is still mostly present at downward end of both trench slopes (Figure 10). Due to the increased width of the flat bed, it takes longer for the sedimentation patches to reach the center of the trench. This only happens after approximately 145 days, while in the Base case this already occurs after around 35 days. In the case with reduced slope steepness (Gentle case), this timescale is unaffected and remains around 35 days. The magnitude of the maximum sedimentation and erosion are similar between the Base and Wide cases. In the Gentle case the maximum sedimentation and erosion rate decrease significantly (Figure 11). Otherwise the patterns are very similar between the two cases (Gentle and Base).

21699011, 2026, 10, Downloaded from https://agupubs.onlinelibrary.wiley.com/doi/10.1029/2025JF008603 by Technical University Delft, Wiley Online Library on [14/10/2026]. See the Terms and Conditions (https://onlinelibrary.wiley.com/terms-and-conditions) on Wiley Online Library for rules of use; OA articles are governed by the applicable Creative Commons License

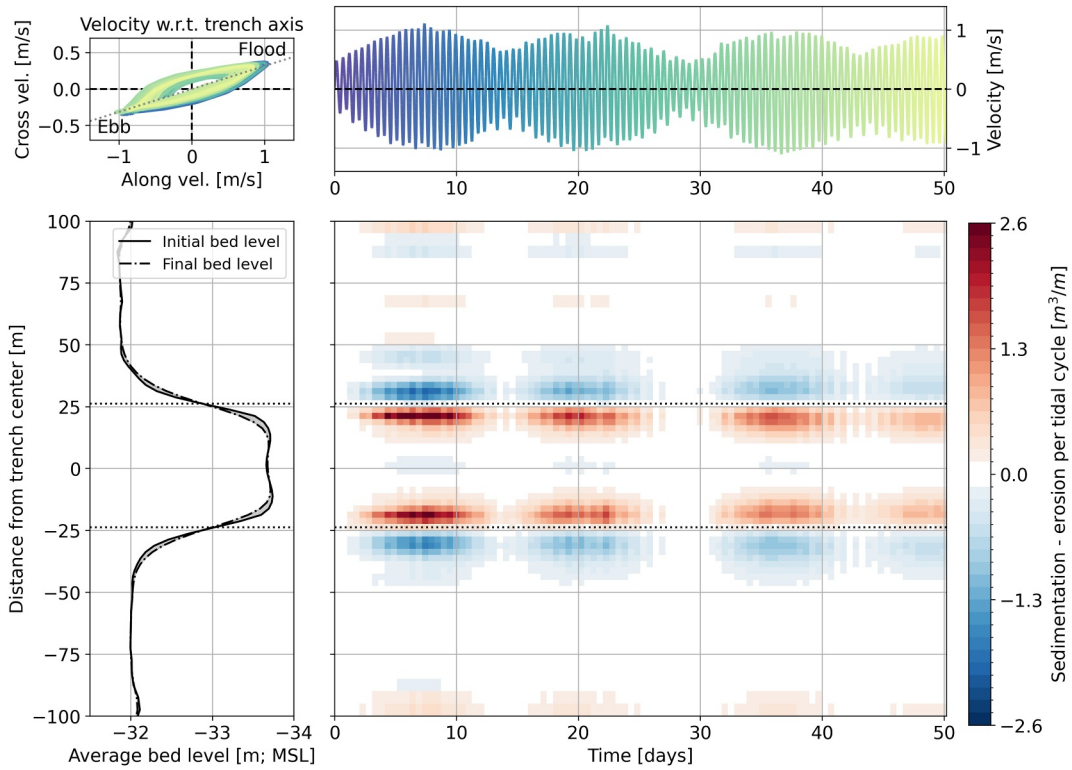


Figure 10. Timestack of along-trench averaged sedimentation and erosion (see Section 2.5) per tidal cycle over the cross trench direction for the first 50 days after dredging with a two times wider trench. Including total velocity magnitude, positive is flood directed (upper), velocity ellipse rotated with trench orientation (upper left) and along-trench averaged bed levels (left). Dotted horizontal lines indicate location of steepest slope.

Comparing the sedimentation volumes over the first 145 days after dredging it is clear that these are mostly influenced by the trench slope steepness and not so much by trench width (Figure 12). With two times gentler slopes the infill volume is lowered by approximately 40%, while with a two times wider trench this volume is only 1% lower with respect to the base case. For the Wide case the peak sedimentation volume is of the same order as in the Base case, but located more outwards from the trench center at the start of the trench side slopes. In the Gentle case these peak volumes have decreased significantly and moved inwards somewhat with respect to the Base case. In both additional cases the dredged volume has increased significantly, with an increase of approximately 60% and 40% for the Wide and Gentle case respectively compared to the Base case. It is thus expected that in both cases the trench will take longer to recover due to the increased dredged volume. Although the initial sedimentation rate is lower in the Gentle slopes case, the Base and Wide cases will reach similar slope steepness and thus reduced infill from the surrounding sand waves in a future stage. In that way the Wide case may develop into a bathymetry alike the Gentle case in the future. It is thus expected that the Wide trench design will take longest to recover even though it has higher initial sedimentation rates.

4. Discussion

In this study we investigated how 3D processes can lead to trench infill and sand wave volume regrowth for a cable trench perpendicular to the sand wave crests, using high resolution 3D Delft3D FM simulations. The simulations show that gravitational, slope-induced amplification, dampening and deflection of bed load transport over the trench side-slopes and vertical, tide-averaged circulation cells play important roles in the recovery of the sand waves. Both processes are highly affected by the surrounding bathymetry. Moreover through long-term simulations we analyzed the temporal variation in trench infill over time and the impact of different trench designs.

21699011, 2026, 10, Downloaded from https://agupubs.onlinelibrary.wiley.com/doi/10.1029/2025JF008603 by Technical University Delft, Wiley Online Library on [14/10/2026]. See the Terms and Conditions (https://onlinelibrary.wiley.com/terms-and-conditions) on Wiley Online Library for rules of use; OA articles are governed by the applicable Creative Commons License

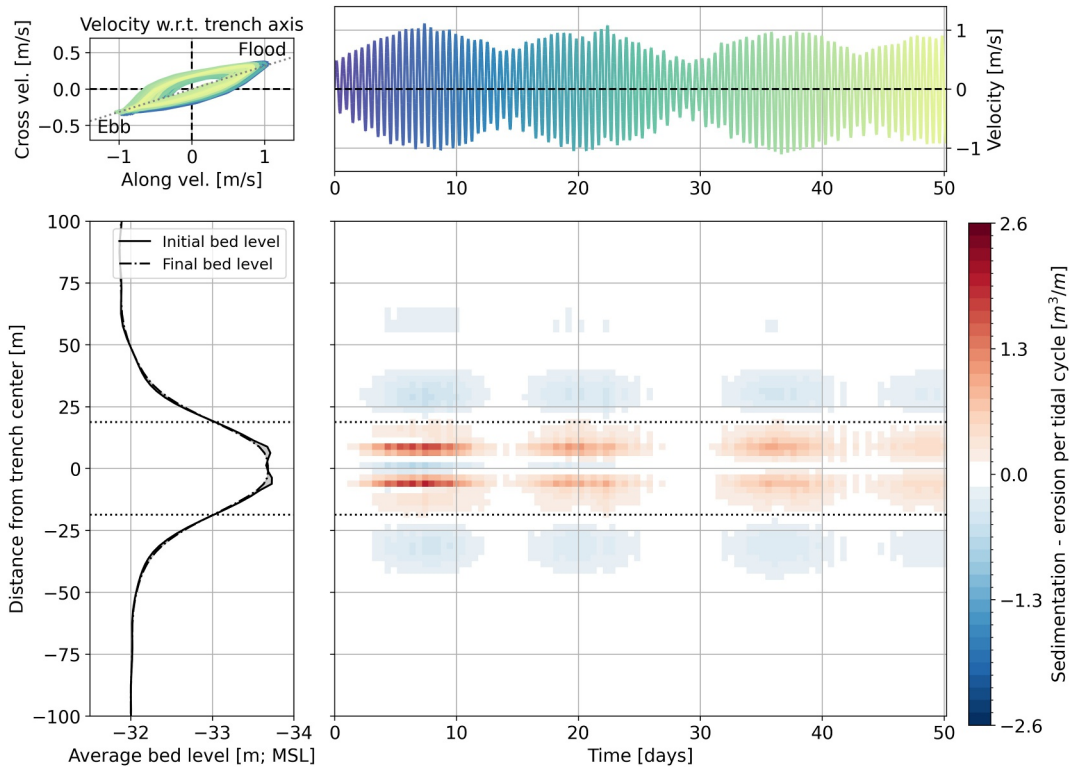


Figure 11. Timestack of along-trench averaged sedimentation and erosion (see Section 2.5) per tidal cycle over the cross trench direction for the first 50 days after dredging with two times gentler trench slopes. Including total velocity magnitude, positive is flood directed (upper), velocity ellipse rotated with trench orientation (upper left) and along-trench averaged bed levels (left). Dotted horizontal lines indicate location of steepest slope.

4.1. Processes Driving Trench Infill and Sand Wave Volume Regrowth

The sedimentation in the trench is mainly caused by gravitational, slope-induced amplification, dampening and deflection of bed load transport over the trench side-slopes. These processes both increases the down-slope transport, while decreasing up-slope transport and deflects the transport direction into the trench. These effects are largest at the location of the steepest side slopes (i.e., next to the crests of the surrounding sand waves). These bed slope effects thus also contribute to volume regrowth of the sand waves, with a fixed crest location next to the surrounding crests. Moreover, depending on the specific orientation of the steepest slope (combining the trench and sand wave slopes) and the currents, these bed-slope effects may theoretically drive regrowth of sand wave crests under an angle with the original crests. Especially for stronger currents, the longitudinal (in flow direction) bed slope effects are leading over the transverse[4] (perpendicular to flow direction) effects, since the transverse component is scaled by the threshold velocity divided by the velocity (see Equation 4), while the longitudinal effects are not. This is confirmed by Figure 6, which shows that the longitudinal slope effects are way more effective in increasing transport rates. Thereby the crests may grow back along the direction of the tidal current, instead of perpendicular to it. This may explain the sideways regrowth observed in Larsen et al. (2020). The fact that this was not observed in the simulation, may be due to the relatively limited current strength or because the crests have broadened in the simulation. Lastly, since especially longitudinal slopes can increase sediment transport rates significantly, the infilling of the trench will occur faster when the trench orientation has a larger angle to the dominant tidal currents. It should be noted that depending on frame of reference the definition of "longitudinal" and "transverse" directions may vary and thereby their respective contributions to trench infill and sand wave regrowth (see e.g., Bailard, 1981).

To further test the importance of bed-slope induced sediment transport, simulations are set up where either or both the longitudinal[4] (in flow direction) and transverse[4] (perpendicular to flow direction) gravitational bed slope effects were excluded, see results in Supporting Information S1. In case both processes are excluded, this means

21699011, 2026, 10, Downloaded from https://agupubs.onlinelibrary.wiley.com/doi/10.1029/2025JF008603 by Technical University Delft, Wiley Online Library on [14/10/2026]. See the Terms and Conditions (https://onlinelibrary.wiley.com/terms-and-conditions) on Wiley Online Library for rules of use; OA articles are governed by the applicable Creative Commons License

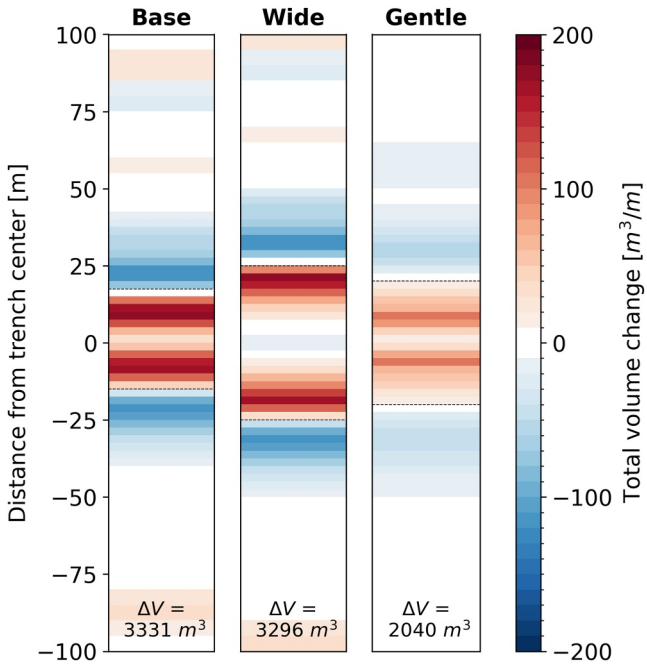


Figure 12. Timestack of along-trench averaged sedimentation and erosion (see Section 2.5) per tidal cycle over the cross trench direction for the first 145 days after dredging, compared between the Base, Wide and Gentle cases. ΔV indicates the total trench infill volume, dotted horizontal lines indicate limits of sedimentation area over which this volume is calculated.

that the bed slope only influences the bed shear stress threshold for sediment transport within the L. C. Van Rijn, 2007 formulation (and thereby the transport magnitude, see L. C. Van Rijn (2007)), but additional magnitude and direction adaptations from Equation 3 and/or Equation 4 are omitted. These simulations highlight the importance of transverse gravitational bed slope effects for trench infill. Without transverse slope effects the initial trench infill, over the first 50 days, is reduced by 75%. By excluding the longitudinal slope effects only a reduction in infill of 10% is observed. Excluding all gravitational bed slope effects only 12.5% (1/8) of the initial trench infill remains. The remaining infill may be caused by the bed slope effects on the threshold for sediment transport, which could not be omitted. In the case without gravitational bed slope effects the intra-tidal sedimentation-erosion pattern completely reverses with the tidal current and shows sedimentation when the current decelerates down the slope and erosion when the current accelerates on the opposing slope. These results show that the longitudinal and (especially) the transverse gravitational bed slope effects and the associated tuning parameters are essential for reproducing trench infill. In this study we have applied default values for both of these tuning parameters. Slightly increasing the parameter for transverse slope effects may lead to a better match for the transverse sediment balance, by increasing the trench infill. With the current trench orientation, the contribution of the longitudinal slope effects to trench infill is limited (see Supporting Information S1). Therefore, reduction of the longitudinal bed slope parameter may lead to better representation of the pointy crests and steep slopes of the sand waves, thereby improving the match between the measured and modeled sand wave height. However, these parameters may wrongfully be used to compensate for other missing or poorly represented processes (Tritthart et al., 2024). Therefore we advise caution in moving away from the default values, which have been determined through extensive experimental studies.

The sediment within the trench is redistributed by the tide-averaged vertical circulation cells (see Figure 5), which cause sand wave regrowth by transporting sediment from the troughs to the crest on both sides. The strength of these circulation cells is usually related to the local sand wave height and steepness and the tidal current strength, but at the location of the flattened trench the currents are amplified under the influence of the surrounding non-dredged sand waves (Figure 13). Thereby, the location and wavelength of the regrowing sand wave is fixed by the surrounding sand waves. Compared to next to the trench, the maximum tide-averaged return current within the trench is reduced by 65%. Of the remaining return current strength only 5% is generated by the local bed undulations. It is expected that with the sand wave recovery the circulation cells will also recover their strength and become more and more locally generated, instead of imposed by the surrounding bathymetry. This suggests that bed slope effects are particularly important during the initial stage of sand wave recovery, while over time the tide-averaged circulation cells may become relatively more important. This is corroborated by the fact that the bed slope effects are actually losing strength over time, due to the flattening of the trench slopes.

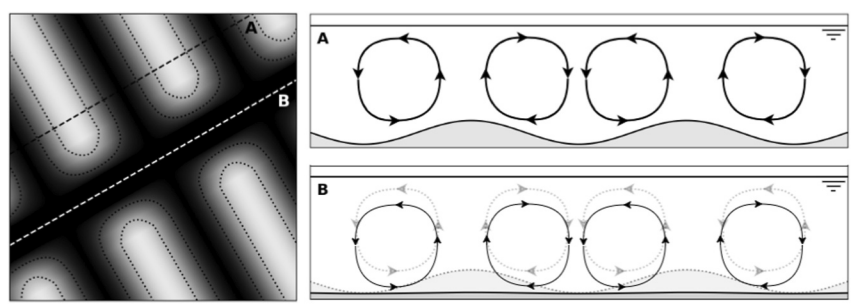


Figure 13. Schematization of the amplification of the tide-averaged vertical circulation cells within a trench.

21699011, 2026, 10, Downloaded from https://agupubs.onlinelibrary.wiley.com/doi/10.1029/2025JF008603 by Technical University Delft, Wiley Online Library on [14/10/2026]. See the Terms and Conditions (https://onlinelibrary.wiley.com/terms-and-conditions) on Wiley Online Library for rules of use; OA articles are governed by the applicable Creative Commons License

21699011, 2026, 10, Downloaded from https://agupubs.onlinelibrary.wiley.com/doi/10.1029/2025JF008603 by Technical University Delft, Wiley Online Library on [14/10/2026]. See the Terms and Conditions (https://onlinelibrary.wiley.com/terms-and-conditions) on Wiley Online Library for rules of use; OA articles are governed by the applicable Creative Commons License

The volume regrowth of sand waves in a cable trench is thus more gradual than predicted by the Landau equation, which has been used to approximate sand wave regrowth rates in a fully dredged case (Knaapen & Hulscher, 2002). This equation predicts slow regrowth at first, due to underdeveloped circulation cells, followed by quick regrowth, which ends asymptotically due to increasing bed slope effects (in the direction perpendicular to the crest). Instead, the amplification of circulation cells within the trench and the bed slope-induced transport at the crest locations will boost the initial sand wave regrowth in the trench. Interestingly, the measurement surveys analyzed by Larsen et al. (2020) also indicate slow initial volume regrowth of the sand wave volume within a cable trench, contrary to the results of this study. This difference may be caused by the mismatch in sand wave height and trench steepness. The height of the sand waves studied by Larsen et al. (2020) is two to three times lower than the sand waves included in this study. This height difference can have a significant effect on the strength of the circulation cells within the trench, while a reduced steepness of the side-slopes may limit slope-induced transport. Additionally, it is observed that the sedimentation starts at the sides of the trench and initially erosion may be observed in the trench center. The determined trench infill volume is thus highly sensitive to the definition of the infill area included in the volume analysis. Finally, it should be noted that the sand wave shape adaptations observed in the model results will slightly affect the strength of both the gravitational bed slope induces transport and vertical current circulation. Through reduced height of the surrounding sand waves both processes are slightly dampened, potentially (partially) explaining the lower infill rates found in the model with respect to the measurements, see Figure 3.

Lastly, the influence of storm-induced currents, for a specific extreme storm event, was investigated. The results show that the total infill rate is hardly affected by these currents due to their dual effect: amplifying one tidal current, while dampening the other. However, due to the resulting asymmetric sedimentation-erosion patterns, the trench may migrate over time due to the residual currents. This offers an explanation for the lateral trench migration observed in Orsted (2018). It should be noted that during these conditions otherwise negligible processes, such as suspended sediment transport and free surface waves, which are not included in this study, may gain importance. Both of these processes are expected to cause additional trench infilling during adverse weather conditions. In calm periods their contribution is expected to be minimal due to limited strength of the tidal current compared to the sediment grain size and the significant water depth compared to the free surface wave height.

4.2. Simulating Morphological Development After Human Intervention

The results show that the high-resolution 3D model is well able to reproduce the multiyear sediment balance of a trenched sand wave. By analyzing the simulation results, we can indicate which processes are vital to recreate this system and where simplifications may be possible to reduce the computational effort. The dominance of bed slope-induced transport and the influence of the surrounding sand waves on the tide-averaged vertical circulation cells verify the need for a 3D setup of the numerical model. Without the cross trench dimension (in a 2DV setup), the trench infill will be lacking from the simulation. In that case even the redistribution of sediment within the trench will be significantly underestimated due to the missing amplification of the circulation cells due to the surrounding sand waves. Moreover, the grid resolution in the cross trench dimension should be high enough to be able to capture the slope steepness of the side slopes and avoid underestimation of the bed slope-induced trench infill. Finally, to accurately capture the vertical current circulation driving sand wave growth, the inclusion of sufficient layers over the vertical is essential. In absence of these vertical layers (in a 2DH model), the sand waves would gradually dampen out. This would reduce sand wave regrowth both due to the absence of vertical current circulation and due to additional dampening of the surrounding sand waves.

The limited importance of storm-induced currents for trench infill, for the considered extreme event, reveals possibilities for simplifying the forcing conditions, especially when there is no clear dominance in the residual current direction. The additional infilling is limited and subsequent storms in opposing directions may balance out the asymmetry in the infill locations. However, it should be noted that these results may not hold for more powerful storms (relative to the tidal strength) and that sand wave migration is likely underestimated when simplifying the forcing conditions (Overes et al., 2024). By simplifying the forcing to a periodical signal, it becomes easier to apply morphological scaling, for example, using the morfac (Ranasinghe et al., 2011). This may significantly reduce the required computational efforts, which in turn can offer opportunities for further investigation of relations between environmental conditions or trench design choices, such as the orientation of the trench with respect to the sand waves, and the trench infill and sand wave regrowth. Since the spring-neap

variation in the tidal signal does have a significant impact on the trench infill volumes and the mobility of sediment within the trench, it is advised to retain this variation in the forcing.

4.3. Practical Implications

The insights gained in this study contribute to understanding and predicting the morphological development of trenched sand waves. The strong spring-neap dependence of trench infill suggests that dredging timing influences the period during which a trench remains open. By timing the dredging activities well with respect to the spring-neap cycle and other local forcing conditions, required dredging volumes can be reduced and more time between dredging and installation, usually carried out with a different vessel, can be achieved. Within the range of trench geometries and environmental conditions considered in this study, the simulations indicate that trench infill rates are more sensitive to side-slope steepness than to trench width. On the other hand, widening the trench is more effective in keeping the sediment away from the trench center, thereby increasing the time horizon for cable installation (in the center). However, in addition to increased dredging volumes, there are other downsides to these design choices. For example, if the trench infill cannot keep up with the sediment redistribution due to tide-averaged circulation in the trench, the sand waves troughs can reach levels below the dredged level, thereby risking cable exposure. Finally, the spatially asymmetric infilling due to storm-induced currents illustrates that under asymmetrical forcing conditions, the location of minimum sedimentation may deviate from the trench centerline. In extreme cases these asymmetrical conditions may even lead to sideways migration of the trench.

Next to the application of the qualitative insights the numerical model can directly be applied to predict trench infill under local environmental conditions and evaluate trench design alternatives for site-specific conditions. Due to the often encountered lack of field data on the recovery of dredging interventions, the numerical model offers an essential tool to gain insight in these systems for which data-driven analysis or data-model hybrid solutions cannot be used. Even with non-calibrated morphological settings the model is able to accurately reproduce the multiyear trench infill and sand wave volume regrowth, although still further improvements are necessary to accurately reproduce sand wave heights. Nevertheless, these types of simulations can support the planning of offshore activities. Trade-offs in trench design (orientation, width, steepness) can be assessed to allow sufficient time for installation, while taking into account the local environmental conditions. Moreover, by gaining insights into the regrowth of sand waves and related future sediment coverage the need for bed protection can be reduced and environmental impact of cable installation can be assessed. Although computationally demanding, such simulations may be justified in situations where uncertainties in trench recovery have significant implications for dredging volumes, installation planning, or bed-protection requirements.

5. Conclusions

The simulations reveal that trench infill is governed primarily by gravitational modification of bed-load transport on trench side slopes. Because transport rates are highest adjacent to the surrounding sand-wave crests, this process simultaneously drives infill of the dredged area and initiates regrowth of sand waves within the trench. Additional regrowth is caused by tide-averaged vertical circulation cells, which redistribute the sand within the trench. Importantly, these circulation cells persist due to the influence of the surrounding non-dredged sand waves. Both processes lead to a fixed location of the regrowing sand wave crests in the trench and raise the need for 3D morphodynamic simulations.

Temporal variations in trench recovery are dominated by the spring-neap tidal cycle, whereas storm-induced currents have only a limited influence on total infill rates in the considered case, although they can generate asymmetric infilling patterns. The simulations further show that trench volume infill rates are highly sensitive to side-slope steepness but only weakly affected by trench width. This indicates that side-slope design is likely a more effective control on recovery rates than trench width.

Comparison with field measurements shows that the multiyear trench infill volumes are captured well by the uncalibrated, brute-force 3D simulation. This shows that these type of simulations can be used to predict the morphological development of trenched sand waves. Moreover, the gained insight into the temporal and spatial variations in the different recovery mechanisms allows for better assessment of trench recovery timescales and the impact of design choices.

21699011, 2026, 10, Downloaded from https://agupubs.onlinelibrary.wiley.com/doi/10.1029/2025JF008603 by Technical University Delft, Wiley Online Library on [14/10/2026]. See the Terms and Conditions (https://onlinelibrary.wiley.com/terms-and-conditions) on Wiley Online Library for rules of use; OA articles are governed by the applicable Creative Commons License

Conflict of Interest

The authors declare no conflicts of interest relevant to this study.

Availability Statement

The input files and results of the numerical simulations are available via (Overes et al., 2026). This data set also contains the local bathymetry of the original trench and those with an adapted design as initial bathymetry files. Moreover, the measured bed level changes used for validating the morphological results are included as well as post-processing code for calculating the transverse sediment balance. The raw bathymetric data used for creating the initial bathymetry and validating the model results can be requested at the Flamish Hydrographic Office (Agentschap Maritieme Dienstverlening en Kust) via (Agentschap Maritieme Dienstverlening en Kust, 2025).

Acknowledgments
This work was supported by the Dutch Ministry of Economic Affairs and Climate via the SITO-IS subsidy. In addition, the authors acknowledge NWO for funding this research through the Footprint project (project number: NWA.1236.18.003). We thank SURF for the support in using the National Supercomputer Snellius. Furthermore, the authors would like to acknowledge the Agentschap Maritieme Dienstverlening en Kust for making the bathymetric available. Lastly, a special thanks is extended to Ad Reniers and Bram van Prooijen, for supervising the MSc students involved in the project (Zeta and Celine), and to the developers of the Delft3D FM model, whose software enabled us to carry out this research.

References

Agentschap Maritieme Dienstverlening en Kust. (2025). Bathymetrische databank [Dataset]. *Vlaamse overheid*. Retrieved from https://www.agentschapmdk.be/nl/hydrografische-data

Bagnold, R. A. (1966). *An approach to the sediment transport problem from general physics*. US Government Printing Office.

Bailard, J. A. (1981). An energetics total load sediment transport model for a plane sloping beach. *Journal of Geophysical Research*, *86*(C11), 10938–10954.

Bao, J., Cai, F., Ren, J., Zheng, Y., Wu, C., Lu, H., & Xu, Y. (2014). Morphological characteristics of sand waves in the middle Taiwan shoal based on multi-beam data analysis. *Acta Geologica Sinica*, *88*(5), 1499–1512. https://doi.org/10.1111/1755-6724.12314

Bloem, C. (2024). *Modelling the impact of residual currents on the interaction between sand waves and trenches in Delft3D FM*. Master's Thesis TU Delft.

Borsje, B., Kranenburg, W., Roos, P., Matthieu, J., & Hulscher, S. (2014). The role of suspended load transport in the occurrence of tidal sand waves. *Journal of Geophysical Research: Earth Surface*, *119*(4), 701–716. https://doi.org/10.1002/2013JF002828

Borsje, B., Roos, P., Kranenburg, W., & Hulscher, S. (2013). Modeling tidal sand wave formation in a numerical shallow water model: The role of turbulence formulation. *Continental Shelf Research*, *60*, 17–27. https://doi.org/10.1016/j.csr.2013.04.023

Campmans, G., Roos, P., Van der Sleen, N., & Hulscher, S. (2021). Modeling tidal sand wave recovery after dredging: Effect of different types of dredging strategies. *Coastal Engineering*, *165*. https://doi.org/10.1016/j.coastaleng.2021.103862

Creane, S., Coughlan, M., O'Shea, M., & Murphy, J. (2022). Development and dynamics of sediment waves in a complex morphological and tidal dominant system: Southern Irish sea. *Geosciences*, *12*(12), 431. https://doi.org/10.3390/geosciences12120431

Damen, J., van Dijk, T., & Hulscher, S. (2018). Spatially varying environmental properties controlling observed sand wave morphology. *Journal of Geophysical Research: Earth Surface*, *123*(2), 262–280. https://doi.org/10.1002/2017JF004322

Damveld, J., Van der Reijden, K., Cheng, C., Koop, L., Haaksma, L., Walsh, C., et al. (2018). Video transects reveal that tidal sand waves affect the spatial distribution of benthic organisms and sand ripples. *Geophysical Research Letters*, *45*(21), 11837–11846. https://doi.org/10.1029/2018GL079858

Deltares. (2016). Morphodynamics of Hollandse Kust (zuid) wind farm zone

Deltares. (2018). The 3D Dutch Continental shelf model-flexible mesh (3D DCSM-FM) setup and validation

Deltares. (2025). Delft3D flexible mesh suite 1D/2D/3D modelling suite for integral water solutions user manual D-Flow flexible mesh

EMODnet. (2024). Emodnet digital bathymetry (dtm 2024) [Dataset]. https://doi.org/10.12770/cf51df64-56f9-4a99-b1aa-36b8d7b743a1

Fredsoe, J., & Deigaard, R. (1992). *Mechanics of coastal sediment transport* (Vol. 3). World Scientific Publishing Company.

Hulscher, S. (1996). Tidal-induced large-scale regular bed form patterns in a three-dimensional shallow water model. *Journal of Geophysical Research*, *101*(C9), 20727–20744. https://doi.org/10.1029/96JC01662

Ikeda, S. (1982). Lateral bed load transport on side slopes. *Journal of the Hydraulics Division*, *108*(11), 1369–1373.

Kernkamp, H., Van Dam, A., Stelling, G. S., & De Goede, E. (2011). Efficient scheme for the shallow water equations on unstructured grids with application to the Continental shelf. *Ocean Dynamics*, *61*(8), 1175–1188. https://doi.org/10.1007/s10236-011-0423-6

Knaapen, M., & Hulscher, S. (2002). Regeneration of sand waves after dredging. *Coastal Engineering*, *46*(4), 277–289. https://doi.org/10.1016/S0378-3839(02)00090-X

Krabbendam, J., Nnafie, A., de Swart, H., Borsje, B., & Perk, L. (2021). Modelling the past and future evolution of tidal sand waves. *Journal of Marine Science and Engineering*, *9*(10), 1071. https://doi.org/10.3390/jmse9101071

Krabbendam, J., Roche, M., Van Lancker, V., Nnafie, A., Terseleer, N., Degrendele, K., & De Swart, H. (2022). Do tidal sand waves always regenerate after dredging? *Marine Geology*, *451*, 106866. https://doi.org/10.1016/j.margeo.2022.106866

Larsen, S., Roulund, A., & Mcintyre, D. (2020). Regeneration of partially dredged sand waves. In *Proceedings of the 9th international coastal sediments conference* (pp. 3026–3039).

Leenders, S., Damveld, J., Schouten, J., Hoekstra, R., Roetert, T., & Borsje, B. (2021). Numerical modelling of the migration direction of tidal sand waves over sand banks. *Coastal Engineering*, *163*. https://doi.org/10.1016/j.coastaleng.2020.103790

Németh, A., Hulscher, S., & De Vriend, H. (2003). Offshore sand wave dynamics, engineering problems and future solutions. *Pipeline and Gas Journal*.

Orsted. (2018). Hornsea project three offshore wind farm Hornsea project three offshore wind farm

Overes, P., Borsje, B., Luijendijk, A., & Hulscher, S. (2024). The importance of time-varying, non-tidal currents in modelling in-situ sand wave dynamics. *Coastal Engineering*, 104480. https://doi.org/10.1016/j.coastaleng.2024.104480

Overes, P., Borsje, B., Luijendijk, A., Reyns, J., & Hulscher, S. (2025). The role of sediment transport processes in shaping offshore sand waves. *Continental Shelf Research*, 105513. https://doi.org/10.1016/j.csr.2025.105513

Overes, P., Borsje, B., Luijendijk, A., Tam, Z., Bloem, C., & Hulscher, S. (2026). Model input and results underlying the publication: "HOW 3D processes drive trench infill and sand wave regeneration after dredging" [Dataset]. https://doi.org/10.4121/6401d3eb-c667-46f3-8c19-78fcdfa38f5f

Pessanha, V., Chu, P., Gough, M., Traykovski, P., & Orescanin, M. (2023). Sand wave migration near the southeastern corner of Martha's Vineyard, Massachusetts, USA. *International Journal of Sediment Research*, *38*(5), 629–642.

21699011, 2026, 10, Downloaded from https://agupubs.onlinelibrary.wiley.com/doi/10.1029/2025JF008603 by Technical University Delft, Wiley Online Library on [14/10/2026]. See the Terms and Conditions (https://onlinelibrary.wiley.com/terms-and-conditions) on Wiley Online Library for rules of use; OA articles are governed by the applicable Creative Commons License

PMSS. (2013). Nemo link environmental statement.
Ranasinghe, R., Swinkels, C., Luijendijk, A., Roelvink, D., Bosboom, J., Stive, M., & Walstra, D. (2011). Morphodynamic upscaling with the MORFAC approach: Dependencies and sensitivities. *Coastal Engineering*, *58*(8), 806–811. https://doi.org/10.1016/j.coastaleng.2011.03.010
Reyns, J., Jagers, B., Ranasinghe, R., Kernkamp, H., & Roelvink, D. (2025). A three-dimensional process-based morphodynamic model on orthogonal unstructured grids for coastal applications. *Coastal Engineering*, 104915. https://doi.org/10.1016/j.coastaleng.2025.104915
Tritthart, M., Vanzo, D., Chavarrías, V., Siviglia, A., Sloff, K., & Mosselman, E. (2024). Why do published models for fluvial and estuarine morphodynamics use unrealistic representations of the effects of transverse bed slopes? *Advances in Water Resources*, *193*, 104831. https://doi.org/10.1016/j.advwatres.2024.104831
Van der Meijden, R., Damveld, J., Ecclestone, D., Van der Werf, J., & Roos, P. (2023). Shelf-wide analyses of sand wave migration using GIS: A case study on the Netherlands Continental shelf. *Geomorphology*, *424*. https://doi.org/10.1016/j.geomorph.2022.108559
Van Gerwen, W., Borsje, B., Damveld, J., & Hulscher, S. (2018). Modelling the effect of suspended load transport and tidal asymmetry on the equilibrium tidal sand wave height. *Coastal Engineering*, *136*, 56–64. https://doi.org/10.1016/j.coastaleng.2018.01.006
Van Landeghem, K., Wheeler, A., Mitchell, N., & Sutton, G. (2009). Variations in sediment wave dimensions across the tidally dominated Irish sea, NW Europe. *Marine Geology*, *263*(1–4), 108–119. https://doi.org/10.1016/j.margeo.2009.04.003
Van Rijn, L. (1993). *Principles of sediment transport in rivers, estuaries and coastal seas* (Vol. 1006). Aqua Publications Amsterdam.
Van Rijn, L. (2006). *Principles of sediment transport in rivers, estuaries and coastal seas: Part 2: Supplement (update) 2006*. Aqua Publications.
Van Rijn, L., Walstra, D., & Van Ormondt, M. (2004). Description of TRANSPOR2004 and implementation in Delft3D-ONLINE.
Van Rijn, L. C. (2007). Unified view of sediment transport by currents and waves. I: Initiation of motion, bed roughness, and bed-load transport. *Journal of Hydraulic Engineering*, *133*(6), 649–667. https://doi.org/10.1061/(ASCE)0733-9429(2007)133:6(649)
Verfaillie, E., Van Lancker, V., & Van Meirvenne, M. (2006). Multivariate geostatistics for the predictive modelling of the surficial sand distribution in shelf seas. *Continental Shelf Research*, *26*(19), 2454–2468. https://doi.org/10.1016/j.csr.2006.07.028

21699011, 2026, 10, Downloaded from https://agupubs.onlinelibrary.wiley.com/doi/10.1029/2025JF008603 by Technical University Delft, Wiley Online Library on [14/10/2026]. See the Terms and Conditions (https://onlinelibrary.wiley.com/terms-and-conditions) on Wiley Online Library for rules of use; OA articles are governed by the applicable Creative Commons License